ADVANCED FUNCTIONAL MATERIALS
www.afm-journal.de

Advances in Engineering Toolkits for Construction of Ultralow Disordered Van der Waals Heterostructures

*Zhujun Huang and Davood Shahrjerdi**

The exploration of emerging quantum phenomena by stacking dissimilar atomic layered materials into van der Waals (vdW) heterostructures has driven the development of layer assembly techniques. Achieving ultralow disorder within these heterostructures is crucial for unlocking their novel physical properties. However, current fabrication methods for designer heterostructures have limitations in throughput, yield, and scalability. Over the past decade, engineering toolkits have evolved to address some of these challenges, but their adoption for fabricating designer heterostructures remains limited. In this review, an overview of these emerging engineering toolkits is provided, and examine their utility and limitations in achieving ultralow disordered heterostructures. It is hoped that the insights from this review article can help guide future research directions on advancing the fabrication process of designer heterostructures.

1. Introduction

Two-dimensional (2D) atomic layered materials have attracted much attention due to their utility in realizing novel electronic systems through arbitrary assembly of various 2D layers into designer van der Waals (vdW) heterostructures. Excitingly, these heterostructures offer unique degrees of freedom such as vertical integration order and horizontal rotational alignment, which are unavailable in conventional heterostructures made through epitaxial growth methods. Such properties make designer heterostructures a versatile experimental platform for fundamental condensed matter physics studies[1–5] and the exploration of novel electronic device concepts.[6–10]

To assess progress, previous review articles have documented various aspects of advancements, broadly categorized into three categories: materials production,[11–19] fundamental physics discoveries,[20–23] and technological applications.[24–28] On one hand, designer structures have significantly advanced in both quality and complexity, driven by their remarkable electronic transport properties. These heterostructures have led to fundamental science discoveries with potential applications in unconventional electronics. Recent review articles have discussed the progress on physics of synthetic electron quantum metamaterials.[20] Moreover, a comprehensive review by Rhodes et al. underscores the crucial role of disorders within the heterostructure in dampening the desired carrier transport necessary for inducing exotic electronic quantum effects.[29] However, progress in this field largely relies on a limited subset of fabrication methods characterized by low throughput, yield, and scalability in dimensions. Critically, only a small area within these heterostructures typically achieves the ultralow disordered quality necessary for revealing novel physical properties.

On the other hand, the improvement of material engineering toolkits has primarily focused on scaling up the dimensions of 2D materials and improving the production yield and throughput of vdW heterostructures. As such, review articles on materials production have mostly delved into various synthesis approaches for 2D materials[11–14,19] and methods for layer assembly.[15–18] While these articles offer valuable guidance on available methods for producing 2D materials and their heterostructures, they often lack extensive assessment of various methodologies for application in creating ultralow disordered heterostructures.

Importantly, the limited adoption of emerging material engineering toolkits in current demonstrations of designer heterostructures with exotic quantum electronic effects indicates both an opportunity and a necessity for advancing material quality. Our review article aims to provide an extensive assessment of various methodologies for application in creating ultralow disordered heterostructures. We discuss both the potentials and current limitations of these emerging 2D material toolkits, providing insights into their strengths and weaknesses through critical analysis. By highlighting the limitations of emerging toolkits, we will suggest potential research directions for improving the fabrication process of ultralow disordered heterostructures. We hope that aspects of this review could also benefit research on scalable fabrication of heterostructures as they hold the potential for realizing unconventional electronic technologies enabled by exotic quantum effects.

This article is organized as follows: Section 2 provides an overview of the vdW stacking technique, focusing on graphene as a model system, which represents the current practice in producing ultralow disordered heterostructures. It also addresses the limitations of this technique, which guides the discussions on

Z. Huang, D. Shahrjerdi
Electrical and Computer Engineering
New York University
Brooklyn, New York 11201, USA
E-mail: davood@nyu.edu

The ORCID identification number(s) for the author(s) of this article can be found under https://doi.org/10.1002/adfm.202314439

DOI: 10.1002/adfm.202314439

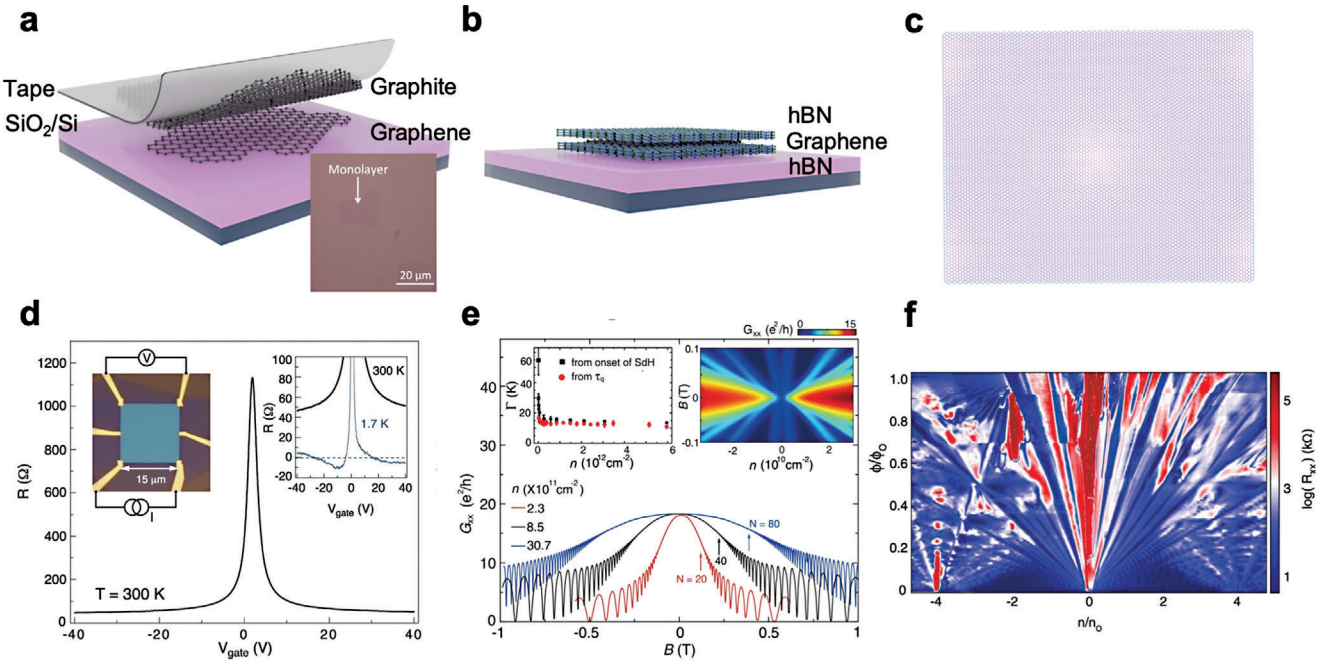

Figure 1. State-of-the-art graphene heterostructures and their performance. a) Schematic of the conventional exfoliation of graphene onto a SiO_2/Si substrate. The inset shows the optical image of a typical monolayer graphene flake obtained via conventional exfoliation. b) Schematic of a BGB heterostructure. c) Schematic of moiré superlattices created by the alignment of graphene and hBN layers. d) Graphene resistance was measured in a van der Pauw structured BGB device at both room and cryogenic temperatures.[31] Negative resistance at 1.7 K indicates ballistic transport over the device's diagonal. e) Magnetoresistance measurement in a Corbino-structured BGB device characterized quantum scattering time and Landau level broadening.[6] f) Magnetoresistance measurement shows the Hofstadter spectrum in a BGB heterostructure where graphene and hBN form superlattices.[32] Inset in (a) reprinted with permission from Ref. [43] Copyright 2015, American Chemical Society. (d) from Ref. [31] Reprinted with permission. Copyright 2013, AAAS. (e) Reprinted with permission from Ref. [6] Copyright 2019, American Physical Society. (f) from Ref. [32] Reprinted with permission. Copyright 2015, AAAS.

the emerging engineering toolkits in Section 3, as they promise to address some of these limitations. However, the emerging toolkits have their own limitations and can generate disorders, which we critically review in Section 4. Section 5 covers techniques for cleaning interfaces, which are instrumental for improving the fabrication process of ultralow disordered heterostructure. Section 6 delves into toolkits for construction of heterostructures involving air-sensitive 2D materials. Section 7 reviews progress on fabricating moiré superlattices. Finally, we conclude by providing our perspective on future research opportunities.

2. Current Practice for Building Ultralow Disordered Heterostructures

2.1. Approach and Benefit

In principle, the construction of vdW heterostructures consists of two main steps. One is the isolation of mono- or few-layer 2D flakes from their bulk parent crystals. Due to the low structural defect density in the bulk crystals compared to their synthetic 2D counterparts, mechanical exfoliation is by far the most practiced method to obtain 2D flakes that exhibit state-of-the-art quantum properties. **Figure** 1a shows the conventional exfoliation using an adhesive tape on a SiO_2/Si substrate.

The second step is the layer transfer of individual 2D flakes to build heterostructures with designed vertical, lateral, and angle alignment. The discovery of hexagonal boron nitride (hBN) marked the boom of research on designer heterostructures. By minimizing substrate-induced Coulomb scattering and potential fluctuation, the use of hBN as the insulating substrate for other 2D materials such as graphene enabled the realization of coherent 2D electron gas systems.[21,29,30] Moreover, the use of hBN flakes as the handle layer atop a polymeric handle layer (discussed in Section 3) has enabled a layer assembly technique, known as vdW stacking. By using an hBN handle layer to transfer 2D flakes, this technique reduces the exposure of the 2D flakes to polymeric stamps, thus enhancing interface cleanliness. Encapsulation in hBN is now the standard practice for modern heterostructures, as illustrated in Figure 1b with the schematic of hBN-encapsulated graphene (BGB) heterostructure.

With vdW stacking technique, the BGB devices have shown carrier mobility on the order of 10^6 cm^2 V^{-1} s^{-1}, corresponding to a mean free path exceeding the device dimensions.[31] Figure 1d illustrates ballistic transport over 20 μm in a BGB device.[31] This fabrication technique has also resulted in significant improvement in the scattering mechanisms in graphene (see Figure 1e).[6] Another remarkable achievement of this technique is the demonstration of the synthetic electronic band structure in graphene/hBN superlattices (see Figure 1c,f).[32] The realization of correlated states in moiré superlattices relies on the strong interlayer coupling at the pristine interface within the heterostructure.

2.2. Limitation

Despite its significant success in enabling numerous scientific discoveries, the vdW stacking technique is not without its practical limitations. As the primary objective of emerging materials toolkits is to overcome these limitations, we now delve into the current fabrication challenges associated with this technique.

Naturally occurring bulk crystals are typically on the order of millimeters. However, the obtained 2D flakes via tape exfoliation are much smaller in size, typically tens of micrometers (see the inset in Figure 1a). In addition to the limited flake size, direct exfoliation onto SiO_2/Si substrates typically results in a small number of mono- or few-layer flakes per exfoliation trial (i.e., low yield, see direct comparison in Ref. [43] and Ref. [47]). Therefore, the production of desired 2D flakes typically requires multiple iterations (i.e., low throughput). These limitations of the conventional exfoliation method have been attributed to the surface roughness of the host substrate and the presence of absorbents on the SiO_2 surface, which weakens the interfacial interactions between 2D flakes and the substrate.

Beyond the limitations of the exfoliation method, another critical issue of the stacking process is the formation of blisters at the newly formed interfaces within the heterostructure. Although hBN as a featureless dielectric protects graphene devices from environmental charged impurities, the construction of atomic-sharp interfaces is not always guaranteed. Surface absorbents could form on 2D flakes during the material preparation and fabrication process. The gaseous, liquid, and solid molecules are likely to be trapped at the vdW interfaces and form nano- or micro-scale bubbles (i.e., blisters) due to the "self-cleaning" mechanism in vdW materials.[33,34] We will return to this topic later to elaborate on the formation of interfacial disorders and the engineering efforts to address this issue in Sections 4 and 5.

3. Engineering Toolkits for vdW Heterostructures Assembly

The above-mentioned limitations pose major barriers to scaling up the dimensions and the fabrication throughput of ultralow disordered heterostructures. Advancing these aspects of the heterostructure fabrication is crucial for promoting new fundamental studies and technological applications by reducing the substantial time and manual labor required to achieve high-quality structures. Therefore, engineering toolkits developed in the past decade share common objectives in one or more aspects of easy production, high throughput, and pristine interfaces for building designer structures.

Drawing from the historical evolution of graphene devices toward quantum coherence, we outline three essential elements for selecting material engineering toolkits to construct low disorder heterostructures. Two key elements include producing ultralow disordered 2D materials and creating pristine interfaces for quantum confinement. The latter is also crucial for promoting interfacial coupling, which enables the interaction of Coulomb fields between charged carriers induced by the proximity of adjacent 2D layers. The final element is the capability to implement designer band structures by creating superlattice heterostructures. These considerations underscore the complexity and precision required in choosing an appropriate fabrication technique for advanced heterostructures. Using these three elements as success metrics, we assess the capabilities and limitations of emerging fabrication techniques in the subsequent sections.

One of the challenges in enhancing the fabrication process of ultralow disordered heterostructures relates to the conflicting interfacial energy requirements between exfoliation and layer assembly. The exfoliation step requires the interfacial energy between the outermost layer of 2D material and the host substrate to exceed the vdW bonding energy within the bulk crystal. In contrast, the subsequent layer transfer step requires the interaction of the exfoliated 2D flake with the host substrate to be smaller than that of the transfer handle layer.

To improve the limitations of the fabrication process, most studies in the literature have generally focused on optimizing either exfoliation or layer assembly, largely independently of each other. Moreover, interface cleaning has gained increased attention in recent years. In the following sections, we will review the emerging engineering toolkits based on their functions, which we classify into three categories: enhancing exfoliation outcome, enabling high-yield layer assembly, and improving interface cleanliness.

3.1. Exfoliation Toolkits

Improving the desired outcome of mechanical exfoliation involves enhancing the interfacial interaction between the outermost layer of vdW materials and the exfoliation surface (e.g., host substrate or exfoliation tape). Key factors for maximizing interfacial interactions include both formation of high interfacial energy and homogeneous contact area. Below we discuss recently developed exfoliation toolkits to improve the exfoliation outcome by engineering these two factors.

3.1.1. Metal-Assisted Exfoliation

Approach and Benefit: Metal films have been implemented as alternatives to adhesive tapes for exfoliating 2D flakes from their bulk crystals.[35–38] To enhance their interfacial energy with 2D materials, the metal-assisted exfoliation techniques employ two different mechanisms. In the first mechanism, a metal film is directly evaporated onto the bulk crystals, serving as a stressor for exfoliating 2D flakes. This metal evaporation process results in a strong binding energy that facilitates the "spalling" in the bulk crystals.[36,37] Subsequently, a backing layer, such as adhesive tape or polymeric film, is deposited onto the metal film to separate 2D flakes from the bulk material (see **Figure 2a**). Moreover, by leveraging the difference in the binding energy between metal and 2D materials, the number of layers within the exfoliated flake can be adjusted by the type or the thickness of the metal film.[37] The resulting flakes exhibit large dimensions on the order of millimeters (see optical image in Figure 2b). This technique has also been used for detaching synthetic 2D layers from their growth substrates, where the 2D layers were produced by epitaxy or chemical vapor deposition (CVD).[39,40]

The other mechanism involves utilizing the smooth surface of a metal film to exfoliate 2D layers from their bulk crystals. In this approach, the metal film is initially deposited

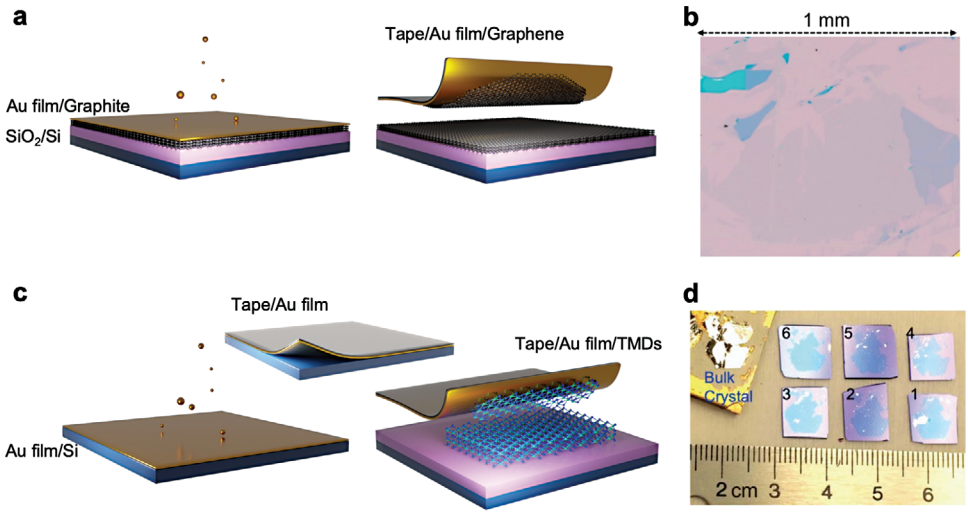

Figure 2. Metal-assisted mechanical exfoliation. a) Schematic of metal-assisted exfoliation of graphene by direct deposition onto graphite crystals. b) Optical image of a representative graphene flake after transferring onto a SiO_2/Si substrate. c) Schematic of metal-assisted exfoliation of TMDs using smooth Au tape. d) Optical image of representative monolayer WSe_2 flakes after transferring onto a SiO_2/Si substrate. (b) reprinted from Ref. [37] CC BY-NC 4.0 (https://creativecommons.org/licenses/by-nc/4.0/). (d) from Ref. [35] Reprinted with permission. Copyright 2020, AAAS.

onto a Si or SiO_2 substrate. Subsequently, a polymeric handle layer is used to peel off the metal film from its host substrate (see Figure 2c).[35] The schematic in Figure 2d shows the exfoliation process of WSe_2 crystal using a gold (Au) film, producing millimeter-size monolayers. Alternatively, this metal-assisted exfoliation can also be performed directly on a metal/SiO_2/Si substrate.[38] The enhanced exfoliation on the metal surface is attributed to the enhanced hybridization between Au atoms and single crystals of transition metal dichalcogenides (TMDs), which exhibits covalent-like quasi-bonding. Theory predicts that the polarized electron density of the noble metal can generate a large dispersion attraction to various 2D materials other than TMDs.[38] However, this same process has minimal impact on improving the exfoliation outcome of graphene and hBN due to their limited adhesion energy with Au.[38]

Limitation: Although metal-assisted exfoliation methods can produce macroscopic-size 2D flakes, they have potential drawbacks. To access the surface of 2D layers for constructing heterostructures, a chemical wet etching process is required to selectively remove the metal film. However, both wet etchants, as well as residual metal particles, can become sources of contamination on the surface of 2D layers. For example, Raman spectroscopy on graphene exfoliated by Au film shows evidence of doping.[37] Lastly, the energetic metal particles generated through evaporation may induce local structural defects within 2D layers during deposition.[41,42] The unintentional incorporation of these disorders can adversely affect the electronic properties of the final heterostructures.

3.1.2. Surface-Enhanced Exfoliation

Approach and Benefit: An alternative approach to enhance conventional exfoliation involves modifying the surface of the SiO_2/Si substrate. Specifically, a previous study has demonstrated that pretreating the SiO_2/Si substrate with oxygen plasma, along with an annealing step during the exfoliation by heating up the host substrate, improves the size of the exfoliated flakes to hundreds of micrometers (see **Figure 3a,b**).[43] This improvement is attributed to the removal of organic absorbents from the SiO_2 surface by oxygen plasma cleaning and the formation of a homogeneous contacting area between 2D materials and SiO_2 during the annealing step.

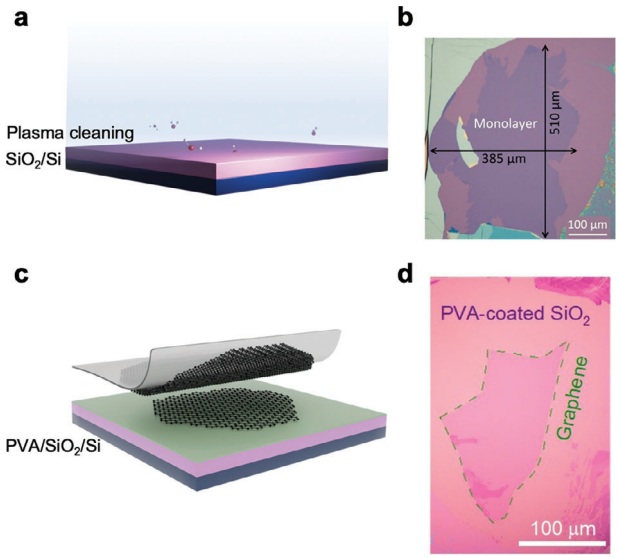

Figure 3. Other exfoliation methods by surface modification. a) Schematic of O_2 plasma treatment to remove small molecule absorbents from SiO_2 surface. b) Optical image of a representative graphene flake. c) Schematic of PVA-assisted exfoliation of graphene. d) Optical image of a representative graphene flake on a PVA-coated SiO_2/Si substrate. (b) reprinted with permission from Ref. [43] Copyright 2015, American Chemical Society. (d) reprinted from Ref. [47] CC BY 4.0.

Limitation: Despite these improvements, the enhanced graphene interaction with the SiO_2 surface hinders the subsequent pick-up of graphene to construct heterostructures.

3.1.3. Polymer-Assisted Exfoliation

Approach and Benefit: One approach to achieve versatile layer transfer involves exfoliating onto a polymer-coated substrate that can later function as the layer transfer handle layer. The implementation of this approach generally involves coating the host substrate with a polymeric stack, consisting of a hydrophobic polymer layer atop a sacrificial polymer layer.[30] When designing these polymer-modified substrates, two factors should be considered. One factor is the polymer concentration, influencing surface smoothness and hydrophobicity to ensure the reliable exfoliation of dry and clean 2D flakes.[44] Another consideration is the thickness of the polymeric stack that should allow optical identification of the exfoliated mono- or few-layer flakes.[45,46]

Previous studies have used polymethyl methacrylate (PMMA) and polypropylene carbonate (PPC) as the hydrophobic layer. Additionally, water-soluble polymers, such as polyvinyl alcohol (PVA) and aquaSAVE, were chosen as the preferred sacrificial layer. Following the exfoliation of 2D flakes onto PMMA or PPC, the sacrificial layer is selectively removed in a water bath, resulting in polymer-supported 2D flakes ready for constructing heterostructures in subsequent layer transfer steps.[30]

It was later discovered that a slight modification of the sacrificial layer could significantly enhance the outcome of the exfoliation step. Figure 3c shows the schematic of this approach, in which exfoliation was directly performed onto an ultrathin PVA film coated on the SiO_2/Si substrate.[47] The substrate underwent a brief annealing process at the glass transition temperature (T_g) of PVA before the exfoliation step, resulting in an improved exfoliation outcome (see Figure 3d). While the exact origin of this phenomenon is unknown, this improvement is attributed to the enhanced interface adhesion between the PVA coating and the graphene layers upon annealing at T_g of PVA. This approach additionally offers the advantage of using the PVA as a sacrificial layer, demonstrating that 2D flake can be directly transferred onto a stamp by locally dissolving the PVA coating underneath the target 2D flake.[47]

Limitation: Although the use of exfoliation of 2D flakes onto PMMA or PPC with water-soluble sacrificial layers facilitated the fabrication of new heterostructures (i.e., graphene/hBN heterostructure[30]), it did not improve the outcome of the exfoliation step when compared to the conventional method. In contrast, the use of the PVA-assisted exfoliation significantly improves the dimensions of the 2D flakes and their production yield. However, this technique poses an additional challenge for achieving ultralow disordered heterostructures by contaminating the 2D flakes with polymeric residues.

In this section, we provided an overview of several alternatives to the conventional exfoliation approach. While these new methods have expanded the exfoliation toolkit, the exposure of 2D flakes to polymer or metal raises concerns about the incorporation of additional disorders that can adversely affect the performance of the resulting vdW heterostructures. Hence, a crucial question to investigate is whether heterostructures created from these 2D layers can achieve comparable performance to their state-of-the-art counterparts. We will revisit this question in Section 5.

3.2. Layer Assembly Toolkits

3.2.1. Approach and Benefit

The choice of the material production method often influences the optimization process of layer assembly. In the case of exfoliated flakes, the vdW stacking is the typical method for assembling individual 2D layers into a heterostructure. Alternatively, 2D flakes, obtained using metal-assisted exfoliation, can be directly transferred onto the target substrate via the metal tape, followed by the chemical wet etch of the metal layer. This step is repeated multiple times to construct the designer heterostructures.

Figure 4a illustrates the simplified schematic of a layer transfer setup, where a polymer stamp is produced for transferring and manipulating 2D flakes. An important consideration of the stamp design is the choice of the polymeric handle layer based on its T_g. Specifically, the handle layer at T_g undergoes a transition from a glassy state to a rubbery state,[48] enabling the temperature control of the viscoelastic property. This attribute serves as a design parameter to facilitate the pick-up or drop-down of a target 2D flake by the stamp.[45,49,50] Figure 4b,c illustrate this concept using PPC as an example of the polymer handle layer, where T_g of PCC is 40 °C. The polymer handle layer is dissolved in an organic solvent upon the completion of the layer transfer process.

To eliminate the exposure of individual 2D layers to solvents, kinetically switchable adhesion of elastomers can be used in the layer assembly process.[51–53] To separate the 2D flake from a substrate, a high lifting velocity of the elastomer is preferred, leading to favorable adhesion of the 2D flake to the elastomer. Conversely, a low lifting velocity of the elastomer promotes favorable adhesion of the 2D flake to the substrate, completing the flake drop-down. Figure 4d shows the measured velocity-dependent adhesion to the elastomer in a rolling experiment.[53] This transfer process is referred to as "all-dry transfer" as it eliminates the need for an organic solvent.[51]

Engineering the shape and geometry of the stamp presents another rich opportunity for enhancing the versatility and effectiveness of the layer transfer process. Stamp designs that reduce the contact area to the substrate could improve the control of the 2D flake manipulation. For instance, a hemispherical-shaped stamp was employed to perform the "tear-and-stack" of a graphene flake (Figure 4e, see Section 7 for details).[54] Other studies have demonstrated the use of a lens-shaped stamp center to facilitate pinpoint accuracy in the "pick-and-place" process,[55] and pyramids-shaped corners to control the contacting area during the "all-dry transfer" process.[52]

Another potential application of stamp design lies in controlling the lamination process. For instance, the hemispherical-shaped stamp permits the engineering of the contact angle at the circumference of the contact area (Figure 4f). The value of the contact angle influences the lamination speed and pressure, which are crucial parameters in the interface cleaning process to squeeze out the air bubbles and other trapped substances at

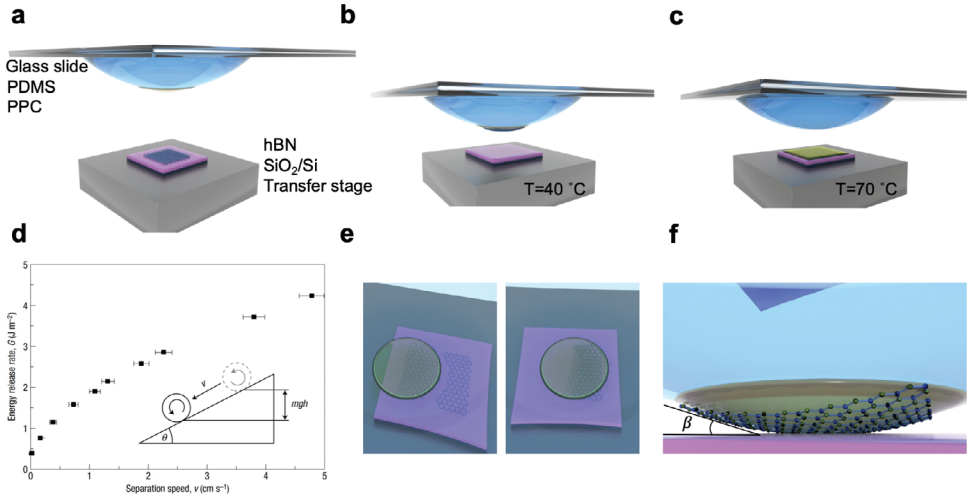

Figure 4. Layer assembly. a) Schematic of the layer assembly setup, which consists of a glass slide, a PDMS base, a PPC handle layer as the stamp, and hBN flake on SiO_2/Si substrate on a transfer stage. b) The hBN layer pickup happens at a stage temperature of 40 °C. c) The hBN layer dropdown happens at a stage temperature of 70 °C while leaving the PPC handle layer together onto the substrate. d) The rate-dependent adhesion as a function of separation speed is measured by a cylinder rolling down an inclined PDMS base. e) Tear-and-stack of monolayer graphene. The tear of graphene is defined by the shape of the handle layer. f) Formation of the contact angle (β) at the lamination front of a hemispherical stamp. (d) reprinted from Ref. [53] with permission. Copyright 2006, Springer Nature.

heterostructure interfaces.[56–58] Nonetheless, an alternative strategy is to employ an inclined substrate to create the contact angle during the layer assembly process.[55]

4. Material Disorders in Heterostructures Built by Engineering Toolkits

Disorders in vdW heterostructures can significantly degrade electron transport. Therefore, it is crucial to understand the sources of disorders and implement strategies for their mitigation to achieve advanced vdW heterostructures. We follow the terminology of a previous review article[29] and categorize various material disorders into two groups: intrinsic and extrinsic. Broadly speaking, intrinsic disorders include the atomic defects within the structure of 2D materials while extrinsic disorders include non-idealities on the surface of 2D layers or interfacial imperfections within the heterostructure. Next, we provide a critical review of disorders that commonly occur when utilizing the recent engineering toolkits discussed in the previous sections.

4.1. Intrinsic Disorders

Scanning tunneling microscopy (STM) has been used to characterize intrinsic atomic defects in exfoliated 2D materials. Exfoliated graphene flakes obtained from commercially available graphite crystals contain mostly point-like defects with a density on the order of 10^8 cm^{-2} (see **Figure 5a**).[59] For exfoliated hBN flakes, STM studies indicate a charged defect density on the order of 10^9–10^{10} cm^{-2} (see Figure 5b).[60] Unlike graphene and hBN, exfoliated TMDs from single crystals show a significantly higher defect density on the order of 10^{13} cm^{-2} (see Figure 5c).[61] This higher defect density is attributed to the lower defect formation energy in TMDs compared to graphene and hBN. Due to its low intrinsic disorder, graphene has served mostly as a model system for studying the effects of extrinsic disorders within heterostructures on electronic carrier transport.

Besides intrinsic atomic defects formed during material synthesis, structural damage can occur during the fabrication process of heterostructures. To be specific, when using a polymeric

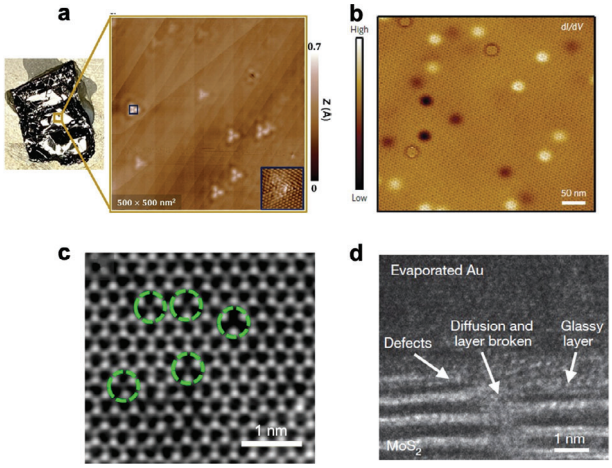

Figure 5. Intrinsic disorders. a) STM topography of point-like defects in graphite. b) STM dI/dV measurement shows charged defects in hBN. c) Annular dark-field scanning transmission electron microscopy image shows vacancies in the mechanically exfoliated monolayer of MoS_2 flake. d) Cross-sectional TEM image shows the bombardment of Au atoms creates structural damage to the MoS_2 layers, including interface diffusion, chemical bonding, and atomic disorders. (a) reprinted with permission from Ref. [59] Copyright 2021, American Chemical Society. (b) reprinted from Ref. [60] with permission. Copyright 2015, Springer Nature. (c) reprinted from Ref. [61] CC BY 4.0. (d) reprinted from Ref. [41] with permission. Copyright 2018, Springer Nature.

handle layer, wrinkles, cracks, and folds are often observed after the layer transfer step. To pick up an exfoliated 2D flake, the handle layer must overcome the interfacial adhesion between the 2D material and the host substrate. However, the lack of sufficiently strong mechanical support can compromise the structural integrity of the 2D layer during the layer transfer process, leading to the formation of wrinkles, cracks, and folds. Moreover, a polymeric handle layer operating at different substrate temperatures undergoes various levels of thermal expansion, potentially contributing to similar structural damage, as well as inducing significant strain variations within the 2D layer.[62] These types of defects can be largely mitigated through careful considerations in the design of experimental procedures.

Another source of process-induced damage is the creation of atomic defects when employing metal-assisted exfoliation. Recent transmission electron microscopy (TEM) studies provide direct evidence that complex defects can form during metal evaporation onto 2D materials (see Figure 5d).[41,42] Hence, caution should be taken when using a metal-induced toolkit for producing 2D layers.

4.2. Extrinsic Disorders

2D materials are susceptible to surface contaminants, posing a significant challenge in producing high-quality vdW heterostructures. These contaminants can get trapped at the interfaces within the heterostructure, resulting in the formation of blisters. **Figure 6a** shows the atomic force microscopy (AFM) image of graphene on hBN heterostructure, illustrating blister formation at random locations. Blisters in heterostructures exhibit diverse characteristics, with sizes ranging from tens of nanometers to a few micrometers and different shapes such as round or pyramidal, suggesting variations of the trapped substances.[33,63–66] Through a combination of topography measurements and elasticity theory predictions, researchers have identified the trapped content mostly as gaseous, liquid, and solid molecules.[33,65,67,68] In this section, we aim to examine the different sources of contaminants and their interaction with 2D materials.

Layer assembly of vdW heterostructure commonly occurs in an ambient environment. The prevalence of absorbed small molecules in the ambient air is intuitively expected to increase the likelihood of their trapping at the heterostructure interfaces. Observation of blisters deflating in a vacuum environment over time or rupturing after a needle jab indicates the presence of gaseous molecules in the blisters.[64] Moisture can be another source of airborne absorbents. In Figure 6b, an AFM image measures the microscopic structure of absorbed water on a graphite surface templated by a graphene film.[69] The density and size of the blisters exhibit a monotonically increasing trend as the relative humidity increases during sample preparation, indicating water vapor as a possible source of blister formation.

Absorption of small hydrocarbon molecules on graphene surfaces due to air exposure has also been studied through high-resolution transmission electron microscopy (HRTEM). Figure 6c illustrates a noticeable surface coverage of hydrocarbon molecules on a pristine graphene surface.[70] In another study, the cross-sectional TEM analysis confirmed the formation of solid blisters due to the aggregation of trapped hydrocarbons at the interfaces.[71] Moreover, this TEM study also revealed that contamination-free regions exhibit an atomic-sharp interface (see Figure 6d).

In addition to the airborne contaminants, 2D materials are likely to be exposed to organic solvents, polymer resists, and metal layers during the fabrication process. For example, PMMA is commonly used for lithographic patterning, and as a handle layer for transferring 2D flakes. Therefore, exposure to PMMA can be a potential source of contamination. In Figure 6e, scanning electron microscopy (SEM) captured a continuous film of polymeric residues on a graphene membrane which was transferred prior by a PMMA handle layer.[70]

Exposure to other polymers can also result in residual contamination. The use of graphene produced via PVA-assisted exfoliation for fabricating BGB heterostructures has revealed a more intricate picture of residual contaminations. Detailed elemental analysis of the HRTEM data not only detected carbon and oxygen elements in the blistered regions but also indicated the presence of silicon elements (see Figure 6f).[56] These findings underscore the strong tendency of 2D layers to absorb various contaminants during the fabrication process of vdW heterostructures.

As discussed earlier, exposure to metals and wet etchant when using metal-assisted exfoliation methods can also introduce additional sources of contamination. Although material characterizations such as Raman spectroscopy and AFM indicate the prospects of these methods, detailed studies investigating the process-induced disorders to an atomic scale within the material and interfaces are still lacking. Further optimization and generalization of the metal-enabled toolkit require a comprehensive understanding of material properties at the atomic level and a thorough evaluation of the electronic transport properties in the resulting heterostructures.

In addition to direct experimental observations of trapped contaminants, computational research has been instrumental in providing new insight into the interactions between 2D materials and various contaminants. Theoretical findings from these studies can serve as a powerful guide in designing the fabrication process by making informed choices regarding the materials for implementing the various engineering toolkits. Figure 6g shows the density functional theory (DFT) simulation results, studying interactions between several small molecules and graphene.[72] These simulations found that small organic molecules such as ethanol, acetone, toluene, and many others mostly exhibit low affinity to graphene surfaces.[72] While bound to the graphene surface, the surface-molecule distance suggests the nature of these interactions is physisorption, which implies easier removal compared with chemisorption molecules.

Similarly, the DFT simulations have been performed to examine the interactions between pristine and defective graphene with PVA molecules (see Figure 6h and Ref. [56]). Remarkably, these simulations found that PVA molecules interact only non-covalently with graphene, even in the presence of highly chemically reactive defects such as monovacancies.

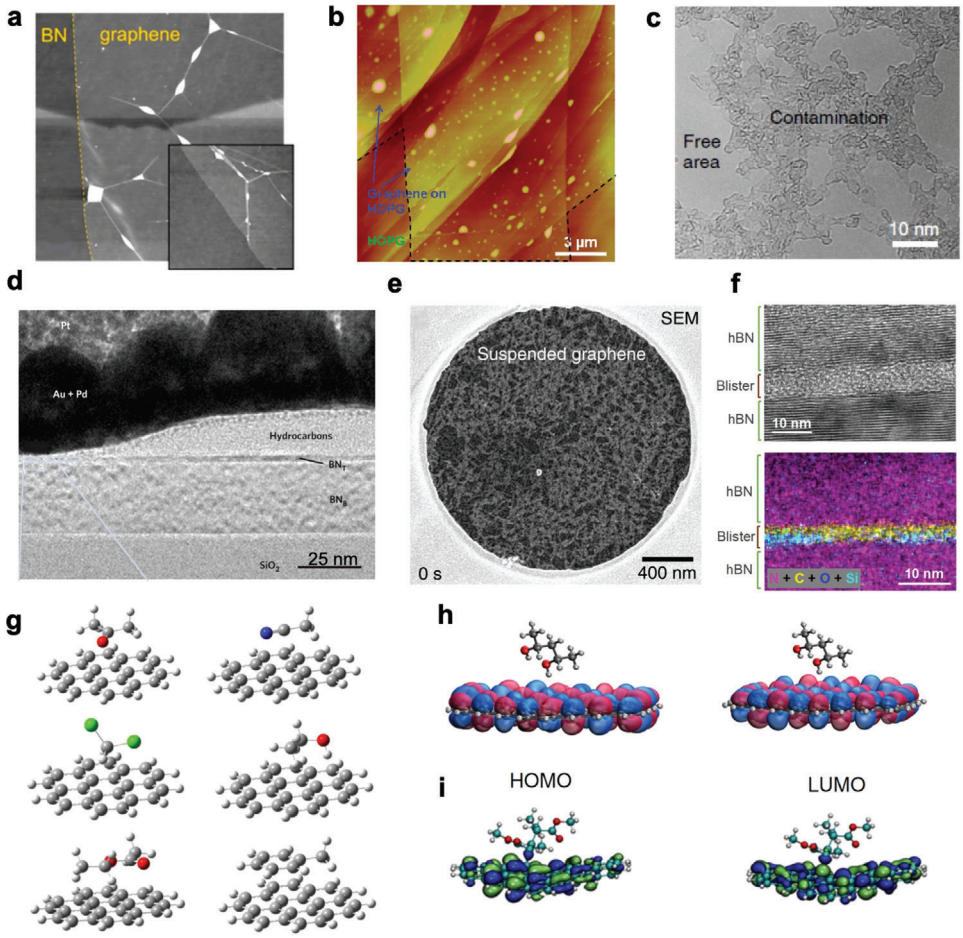

Figure 6. Extrinsic disorders. a) AFM topography of blisters formation at graphene/hBN interfaces. AFM window size is 15 μm by 15 μm. The inset window size is 1.5 μm by 1.5 μm. b) AFM topography of moisture absorbents trapped at the graphene/graphite interfaces. c) HRTEM image of airborne contaminants absorbed onto the graphene surface. d) Cross-sectional TEM image of a blister at graphene/hBN interface indicating hydrocarbons are the main component. e) An SEM image shows a film of PMMA residues on the graphene surface. f) HRTEM image and elemental analysis show that blister consists of hydrocarbons and Si components. g) DFT calculation of interactions between small organic molecules and graphene, including acetone, acetonitrile, dichloromethane, ethanol, ethyl acetate, and toluene. h) DFT calculation of the highest occupied molecular orbitals (HOMO) and the lowest unoccupied molecular orbitals (LUMO) between PVA molecule and graphene. i) DFT calculation of HOMO and LUMO between PMMA molecule and single vacancy graphene. (a) reprinted with permission from Ref. [34] Copyright 2014, American Chemical Society. (b) reprinted with permission from Ref. [69] Copyright 2011, American Chemical Society. (c), (e) reprinted from Ref. [70] CC BY 4.0. (d) reprinted from Ref. [71] with permission. Copyright 2012, Springer Nature. (f), (h) reprinted with permission from Ref. [56] Wiley. (g) reprinted with permission from Ref. [72] Copyright 2013, American Chemical Society. (i) reprinted from Ref. [74] CC BY 4.0.

In contrast, other theoretical studies have demonstrated that PMMA radicals form covalent bonds with defective graphene (see Figure 6i).[73,74] These findings support the experimental observation that PMMA residues cannot be fully removed from graphene surfaces even after excessive thermal annealing.[73]

In this section, we covered the potential challenges associated with the emerging engineering toolkits for producing ultralow disordered heterostructures. Both intrinsic and extrinsic disorders were discussed, given their significant impact on accessing intrinsic physics properties of 2D materials. Hence, careful attention to these pitfalls is essential when selecting an engineering toolkit for realizing advanced heterostructures. In the following section, we discuss potential remedies for mitigating extrinsic disorders.

5. Engineering Toolkits for Cleaning Heterostructures

In this section, we review the methods to reduce the surface contaminants of individual 2D layers. We will also describe current methods for cleaning interfaces within the heterostructures.

5.1. Thermal Decomposition of Contaminants

5.1.1. Approach and Benefit

Annealing 2D layers at elevated temperatures is a common method for decomposing organic contaminants and removing surface impurities. The effectiveness of this cleaning method

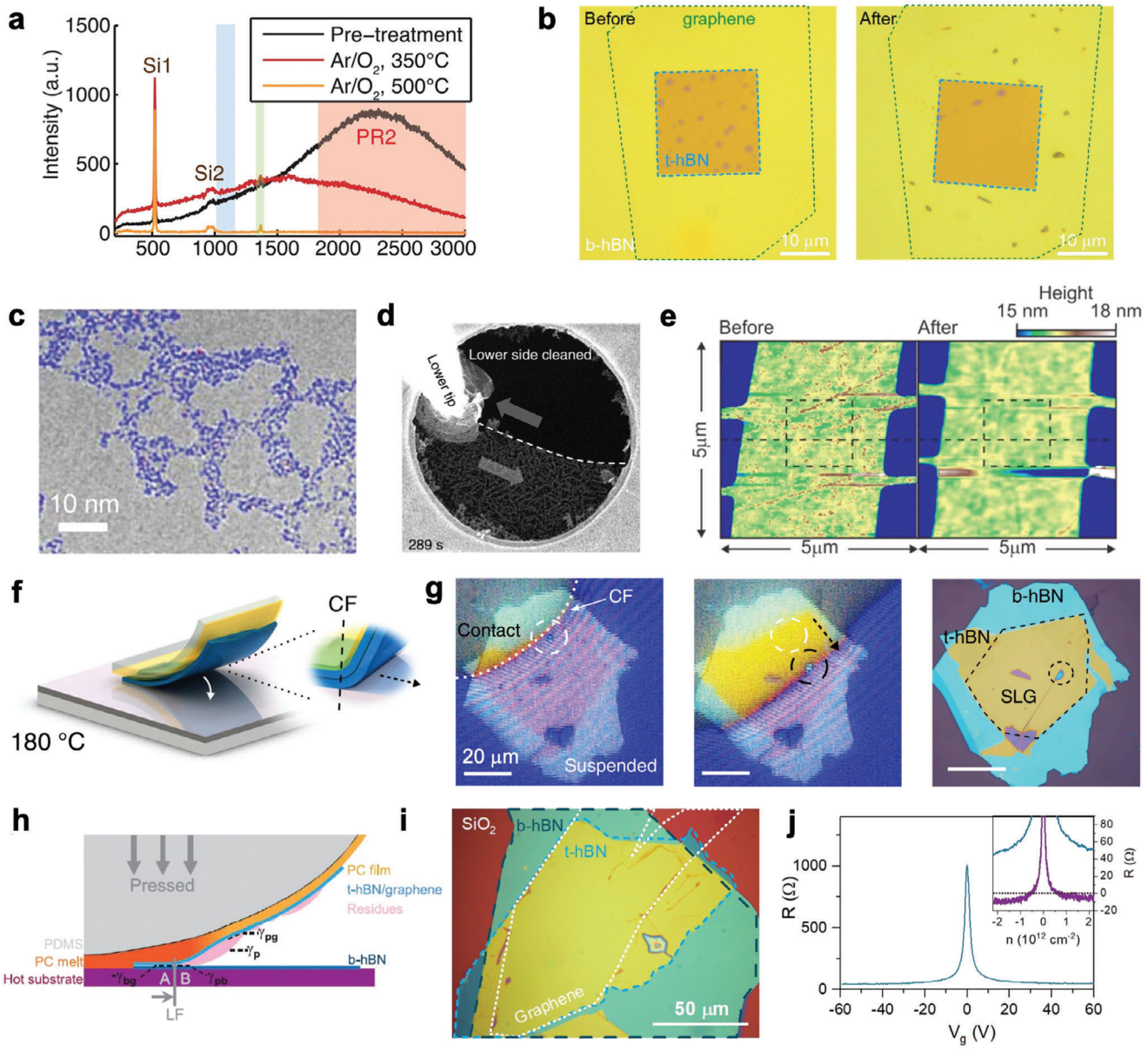

Figure 7. Cleaning heterostructures. a) Raman spectroscopy of hBN before and after annealing in Ar/O_2. b) Optical images of a BGB heterostructure before and after vacuum annealing. c) SEM image of PMMA residues on graphene surface after thermal annealing. d) In situ SEM imaging of mechanical cleaning of PMMA residues on graphene using a fine-metal tip. e) Optical images of a BGB heterostructure before and after AFM ironing. f) Schematic of lamination cleaning of a fully formed BGB heterostructure, and recordings of the interface cleaning process. h) Schematic of the interface cleaning mechanisms. i) Optical image of the fully cleaned BGB heterostructure built using polymer-contaminated graphene. j) Electrical measurement of BGB heterostructure built using polymer-contaminated graphene showing ballistic transport at 1.5 K. (a) reprinted with permission from Ref. [75] Copyright 2012, American Chemical Society. (b) reprinted from Ref. [47] CC BY 4.0. (c) reprinted with permission from Ref. [73] Copyright 2012, American Chemical Society. (d) reprinted from Ref. [70] CC BY 4.0. (e) reprinted from Ref. [81] CC BY 4.0. (f), (g) reprinted from Ref. [57] CC BY 4.0. (h)-(j) reprinted with permission from Ref. 56] Copyright 2022, Wiley.

strongly depends on the annealing ambient. For example, a study has shown that prolonged annealing in Ar/H_2 is ineffective in removing polymeric residues from exfoliated hBN flakes.[75] Raman spectroscopy shows a broad photoluminescence background, originating from the remaining organic residues (see **Figure** 7a).[75] In contrast, a modified annealing recipe in an O_2 ambient was shown to be effective in removing the organic residues from hBN flakes.

Beyond cleaning the surface of individual 2D layers, annealing has been employed to remove blisters in fully formed heterostructures both pre- and post-device fabrication.[2,32,47,76–78] Figure 7b illustrates the reduction of blisters in a BGB

heterostructure upon annealing.[47] The annealing process appears to have activated the movement of blisters, resulting in the interfacial cleaning of the heterostructure.

5.1.2. Limitation

The annealing approach to clean individual 2D flakes requires careful consideration of the annealing ambient. For example, although an O_2 ambient is efficient for removing organic contaminants, it cannot be used on some 2D materials like graphene, TMDs, and air-sensitive materials, as these materials are prone to oxidation. Annealing in an inert environment like the ultrahigh vacuum (UHV) is more suitable for cleaning such 2D layers.[73,79,80]

Moreover, the outcome of the cleaning process is also influenced by the strength of molecular interaction between the organic contaminants and the 2D materials. The experimental results of using thermal annealing for removing PMMA residues from the graphene surface are far from satisfactory (see Figure 7c). The PMMA residues undergo a two-stage decomposition during which the PMMA radicals react with graphene defect sites and form covalent bonds.[73] Such interactions permanently compromise the quality of 2D layers and limit their use in fabricating advanced heterostructures.

The annealing method is also unsuitable for cleaning interfaces within heterostructures. The random movement of blisters within the stack is a limitation of this approach. To be specific, blisters could either segregate into bigger bubbles or move out of the heterostructure. This randomness limits the yield of the annealing outcome and prevents the production of clean interfaces across the entire dimensions of the BGB heterostructure.

5.2. Physical Removal of Contaminants

5.2.1. Approach and Benefit

Applying mechanical force to contaminants has been shown to be effective in cleaning the surface of 2D layers and interfaces within heterostructures. Figure 7d shows the mechanical removal of PMMA residues on a suspended graphene film using a fine metal tip.[70] It was confirmed by in situ imaging that one can achieve complete cleanliness of monolayer graphene film by this mechanical cleaning method. However, the contaminants are almost immediately formed on the surface again upon exposure to air (see Figure 6c).

Other studies implemented an AFM-based technique, called AFM ironing, for cleaning fully fabricated BGB heterostructures.[81,82] The stack topography showed improved surface roughness, suggesting enhanced interlayer coupling and heterostructure homogeneity (see Figure 7e). The superior quality of the heterostructures was also confirmed by enhanced carrier mobility in graphene in these studies.

5.2.2. Limitation

The mechanical cleaning approach is limited to small areas, making it challenging to scale up to produce large-area atomic-sharp heterostructures.

5.3. Directional Blister Removal

5.3.1. Approach and Benefit

Achieving blister-free interfaces across the entire dimension of BGB heterostructures requires a method for directional removal of blisters. A combination of thermal and mechanical actuation has proven to be effective in heterostructure interface cleaning. Two independent studies have demonstrated the large-area interface cleaning in BGB heterostructures by integrating a high-temperature lamination step into the standard layer assembly process.

The first study employed high-temperature lamination on fully fabricated BGB stacks by the vdW stacking method where only airborne contaminants were incorporated.[57] Figure 7f shows the schematic of the cleaning process, performed at 180 °C. The optical images in Figure 7g demonstrate the directional movement of blisters in the fully formed BGB stack, being pushed out of the heterostructure. This approach produced a BGB heterostructure with clean regions approaching 5000 μm^2. Graphene transport characterization shows carrier mobility on the order of 10^6 $cm^2V^{-1}s^{-1}$ at 9 K.

Another study focused on developing a high-temperature lamination method for cleaning BGB heterostructures made from polymer-contaminated graphene.[56] In this study, graphene was prepared by exfoliating on a PVA-coated SiO_2/Si substrate. This study examined the interface cleaning from an energy standpoint, considering that PVA molecules do not form covalent bonds with graphene. It was hypothesized that the mobilization of the polymer residues together with the mechanical actuation can result in the removal of contaminants during the lamination. Figure 7h shows the schematic of the proposed cleaning mechanism. The directional propagation of the lamination front guided the removal of the interfacial contaminants, resulting in BGB heterostructures with a record clean area of 7500 μm^2 (see Figure 7i). Excitingly, this study demonstrated that BGB heterostructures using this cleaning method can achieve ballistic transport with a mean-free path of over 20 μm (see Figure 7j). These results are equivalent to the state-of-the-art BGB devices, fabricated using the vdW stacking process (Figure 1d).

5.3.2. Limitation

The interface cleaning process in Ref. [57] is primarily effective for cleaning graphene prepared using conventional exfoliation, i.e., graphene was not intentionally exposed to organic solvents or polymeric contaminants. However, applying the same process (at 250 °C) to BGB heterostructures made from PMMA-contaminated graphene had limited success, illustrating the limitation of this technique in cleaning heterostructures made from polymer-contaminated graphene.

The current demonstrations of the above-mentioned directional blister removal techniques have so far focused on a limited subset of heterostructures, such as BGB or hBN-graphene-MoS_2 stacks.[56] The utility of these techniques for fabrication of more complex heterostructures like moiré superlattices is yet to be

explored. As we will discuss in Section 7, these heterostructures are susceptible to high-temperature processes as well as heterostrain induced by the lamination process.

5.4. Fabrication in Controlled Environments

5.4.1. Approach and Benefit

Exposure of 2D layers during exfoliation and subsequent layer assembly to ambient air can introduce residues like hydrocarbons, leading to blisters formation in heterostructures. Therefore, a common approach is to prevent the exposure of 2D layers to airborne contaminants during heterostructure fabrication. Many research labs achieve this by conducting layer assembly in an inert gas-filled glovebox environment.[16,83,84] Recent studies also demonstrated layer assembly in a UHV chamber, effectively minimizing all potential airborne contaminants.[85] Furthermore, to utilize the UHV setup, researchers developed a layer assembly process by substituting a polymer handle layer with an inorganic film.[86] This aims to prevent polymer outgassing and minimize potential organic contaminants.

5.4.2. Limitation

These specialized layer-assembly chambers often integrate the entire fabrication steps in situ, including mechanical exfoliation, stacking, and material characterization like AFM or Raman spectroscopy. As such, the implementation of these chambers is costly and increases the complexity of the fabrication process. Additionally, fabrication in a glovebox or UHV chamber also restricts the choice of stamp materials to anhydrous polymers and solvents or inorganic films. With their significant cost and complexity, these systems have their highest impact on fabricating heterostructures from air-sensitive 2D materials (Section 6) or constructing moiré superlattices (Section 7).

6. Air-Sensitive vdW Materials

In the broad library of 2D materials, many can be mechanically cleaved down to the monolayer limit. Among these materials, only a handful of them in monolayer form are identified as chemically inert and stable under ambient conditions, such as graphene, hBN, and several TMDs.[12] Indeed, many 2D materials are air-sensitive, undergoing significant degradation of their structural and electronics properties upon exposure to air. A few prominent examples of such materials are black phosphorus (BP, direct bandgap 2D semiconductor),[87–90] $NbSe_2$ (2D superconductor),[91,92] and $MoTe_2$ (rich 2D topology phases).[93–95] Understanding the degradation mechanisms of these materials is essential for developing fabrication strategies that preserve their inherent properties.

6.1. Degradation Mechanisms

The primary mechanism contributing to material degradation upon ambient exposure is oxidation, which occurs through interactions with oxygen, water, or alkyl segments present in the air. Significant progress has been made in understanding the oxidation mechanisms and its effects using both theoretical modeling and experimental studies.

TMDs are characterized by a chemical formula of MX_2, where M is a transition metal like Mo, W, and X denotes a chalcogen like S, Se, or Te. The choice of M and X significantly impacts the susceptibility of TMDs to oxidation. Typically, selenides are more susceptible to oxidation than sulfides. Exfoliated selenides have been reported to show surface protrusions after ambient exposure. Moreover, transistor study based on WSe_2 has shown that short-term exposure to air generate reversible degradation due to physisorption of water onto WSe_2 pristine surface. However, prolonged exposure to air results in permanent degradation due to chemisorption of O_2 at Se vacancies.[96] Unlike sulfides and selenides, tellurides suffer more severely from oxidation, where Te desorbs both on basal and edge planes.[97] It has been observed that single layer $MoTe_2$ degraded quickly within a few minutes of the exfoliation process[98] (see **Figure 8a**). Regarding the choice of M, theoretical studies indicate that oxygen gains more electron from WX_2 than MoX_2, thereby promoting its oxidative interactions with WX_2.[99]

Atomic defects also affect the oxidation process. Exfoliated sulfides such as MoS_2 and WS_2 are typically air stable on their basal plane due to a low density of defects.[100] However, CVD-grown MoS_2 and WS_2 are prone to aging after long-term exposure to air, particularly at sites rich in chalcogen vacancies, grain boundaries, and edges.[99]

Another widely studied 2D material is BP. Upon exposure to air, small bubbles appear rapidly on the surface with uniform distribution. After a few hours to days, these small nucleation sites accumulate into large droplets, eventually completing the transformation into phosphoric acid (Figure 8b,c).[87,101,102] Further investigations have found that BP does not directly interact with either dry oxygen or water. Under normal conditions, light-induced excitons can initiate chemical reactions between BP and oxygen.[87] Alternatively, the water polarization effect can assist electron transfer between BP and oxygen, causing the pristine BP surface to transition from hydrophobic to hydrophilic, as shown in Figure 8d.[102] Furthermore, water molecules attract O-P bonds and eventually remove P by hydrogen bonding, resulting in the dissolution of the top layer and further oxidation.[99] Crucially, a similar mechanism (i.e., water-assisted oxidation) has been observed on other 2D materials as well, such as InSe,[103,104] WSe_2.[96]

The oxidation behavior of 2D materials varies. The mechanisms described above primarily occur in a layer-by-layer manner due to the absence of dangling bonds on the pristine material surface. In contrast, some 2D materials are reported to exhibit anisotropic degradation. For example, the degradation of ferroelectric $NbOI_2$ is dominated by unstable dangling iodine bonds on the (100) plane along c-axis (see Figure 8e).[105] Despite progress on this topic, further research is needed to explore the full spectrum of oxidation behavior in various 2D materials, which will be crucial for their practical applications in emerging technologies.

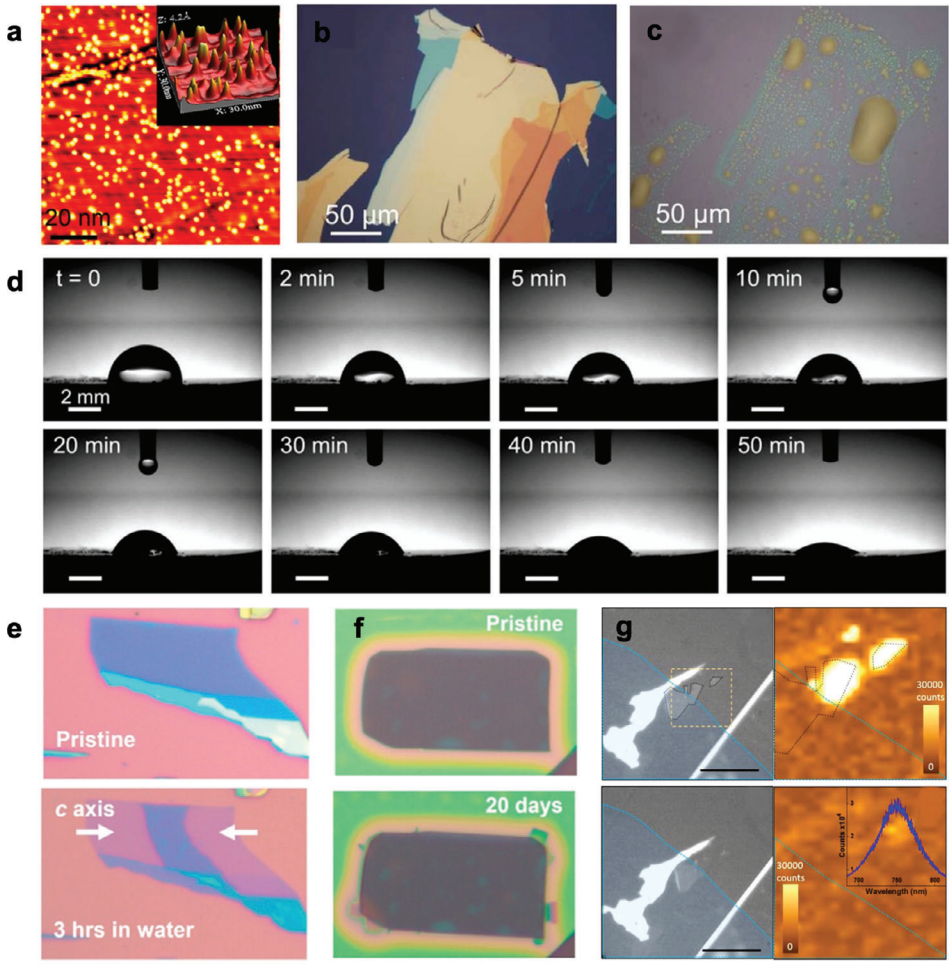

Figure 8. Air-sensitive materials. a) A typical STM image of a freshly exfoliated $MoTe_2$ flake. Randomly distributed protrusions are observed on the surface, with an average height of 3 Å. b) Optical images of freshly exfoliated BP and c) after exposure to air for a week. d) Contact angle of water drops on the surface of BP, illustrating a transition from hydrophobic to hydrophilic upon aging. Scale bar 2 mm. e) Optical images of $NbOI_2$ flake shrinks on the (100) plane along c-axis after 3 h water exposure. f) hBN-encapsulated $NbOI_2$ flake shows no obvious change after 20 days. g) Partially encapsulated bilayer BP by hBN shows no degradation in the encapsulated region and complete degradation in the exposed region. Right panels show the corresponding photoluminescence measurements. (a) Reprinted with permission from Ref. [98] Copyright 2017, American Chemical Society. (b)-(d) Reprinted with permission from Ref. [102] Copyright 2016, American Chemical Society. (e,f) Reprinted with permission from Ref. [105] Copyright 2024, American Chemical Society. (g) Reprinted with permission from Ref. [89]. Copyright 2015, American Chemical Society.

6.2. Fabrication Strategies

Various techniques have been developed to protect air-sensitive 2D materials from the reactive oxygen species and preserve their intrinsic properties. Common practices include the application of capping layers made of 2D material such as hBN or graphene,[89,106] ALD oxides,[88] anhydrous polymeric film such as parylene-C,[87,107] or ionic liquid.[90] However, the formation of ALD oxides requires an oxidative precursor like water or oxygen radicals, which can contribute to the oxidation of the 2D material. Moreover, the use of oxide and polymeric film as an encapsulation layer could induce interface charges and degrade electronic properties. Alternatively, oxidation of the topmost layers has been used to cap the underlying layers.[88,108,109] Applying a similar strategy to β-FeSe has been shown to enhance the superconducting critical temperature, primarily due to the reduced thickness.[108]

Despite the achieved improvements, these techniques fall short of fully harnessing the inherent properties of 2D materials. This shortcoming outweighs the attempts by these techniques to simplify the fabrication process. Currently, hBN encapsulation is the most effective approach for preserving the intrinsic properties of air-sensitive materials (see Figure 8f,g).[8,89,103,105] Furthermore, fabrication under a controlled environment as described in Section 5.4, such as a glovebox, remains the preferred toolkit for this group of 2D materials.

7. Moiré Materials

This section gives a brief overview of the fabrication process required to construct complex designer structures, specifically moiré superlattices. It highlights key developments in the field and the additional challenges involved in fabricating these structures due to their intricate nature, such as rotational alignment.

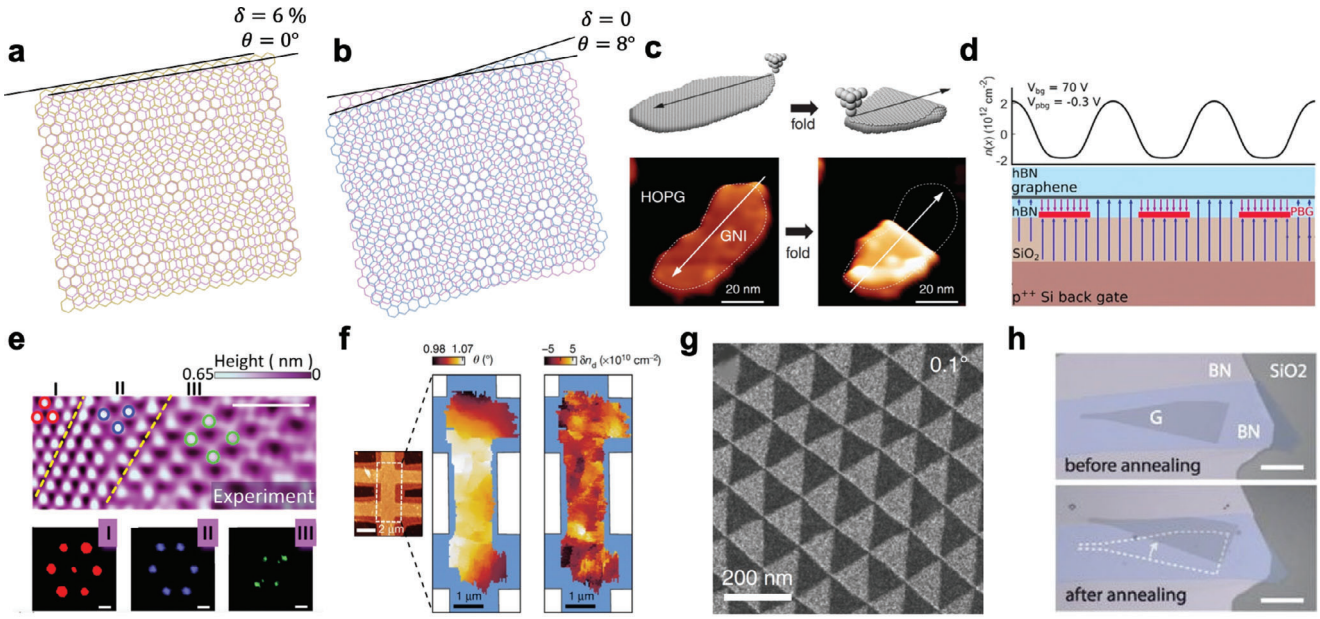

Figure 9. Moiré materials. a) Schematic of moiré heterobilayer with rotational alignment and lattice mismatch of 6%. b) Schematic of moiré homobilayer with 8° relative rotation and no lattice mismatch. c) Schematic and experimental realization of folding graphene nano-island (GNI). d) Schematic of a graphene device on nanolithographically-patterned graphite gate electrode. e) STM topography of t-BLG with different moiré superlattices induced by heterostrain. f) 2D map of the twist angle θ and corresponding charge disorder map in the device area. g) TEM dark field image in t-BLG. The alternating contrast shows AB/BA domains reconstructed from twist angle of 0.1°. h) Angle relaxation after thermal annealing that aligned the edges of graphene and hBN. (c) from Ref. [125] Reprinted with permission. Copyright 2019, AAAS. (d) Reprinted with permission from Ref. [128] Copyright 2020, American Chemical Society. (e) Reprinted from Ref. [132] Copyright 2018, American Physical Society. (f) Reprinted from Ref. [135 with permission. Copyright 2020, Springer Nature. (g) Reprinted from Ref. [140] with permission. Copyright 2019, Springer Nature. (h) from Ref. [32] Reprinted with permission. Copyright 2015, AAAS.

7.1. Fabrication Strategies of Moiré Materials

Moiré materials occur in an electronic matter that shows periodic structure comparable to the electron wavelength. The strong interactions between electrons in the subwavelength structures lead to various interesting physics, which drives the research on the development of new moiré superlattices. 2D materials are of significant interest in designing new moiré superlattices due to their layer-by-layer structure, facilitating the manipulation of electronic states in individual atomic layers. At present, experimentalists engineer the spatial wavelength of moiré superlattices using one of these strategies: the lattice mismatch (δ) between layers, rotational alignment (θ) between layers, and lithographical patterned substrate. Following this classification, we discuss in this section the strengths and limitations of each fabrication strategy.

Category 1. A heterobilayer moiré superlattice forms when two different 2D materials with a small lattice mismatch are stacked while maintaining their angle alignment (see **Figure 9a**). Prime examples of such superlattices include graphene on hBN, which exhibits fractal Hofstadter spectra,[3,4,32,110] rhombohedral-trilayer graphene (r-TLG) on hBN,[111–113] and heterobilayers of TMDs.[93,95] To fabricate the heterobilayer structure, the edges of two different flakes are often aligned optically. This approach relies on the tendency of 2D materials to fracture along the crystallographic direction.[114,115] Although the optical method provides a good guide for the crystal axis, it may not offer sufficient precision when extreme control of the alignment rotation is required. To achieve high precision, an alternative approach is to predetermine the crystal axis or the preferred domain (ABC domain in r-TLG) using non-destructive optical measurements before layer assembly. However, this strategy requires special instrumentation, such as angle-resolved second harmonic generation,[116–118] Raman spectroscopy,[119,120] and scanning near-infrared microscopy.[121]

Category 2. Homobilayer moiré superlattices are constructed by introducing a small relative angle rotation between two layers of the same material (see Figure 9b). A prominent example within this category is twisted bilayer graphene (t-BLG), known for exhibiting a flat band at a small rotational misalignment of 1.1°.[122,123] The current practice for fabricating these structures involves the "tear-and-stack" method. In this approach, an hBN flake partially contacts a graphene flake and tears the contacted part. Then, the entire stamp with the hBN/graphene stack moves over to the remaining graphene, with a small relative angle created by the stage rotation and picks up the second half of the graphene (as depicted in Figure 4e). This method can, in principle, be extended to create relative twist angles between any number of layers, for example, twisted trilayer graphene.[124] This approach produces high-quality moiré superlattices with excellent carrier transport properties. However, the reproducibility and homogeneity of small-angle rotation pose challenges. We will discuss angle disorders in Section 7.2. Another approach to creating t-BLG involves folding a

single-layer graphene flake (see Figure 9c). This implementation utilizes an STM or AFM tip to pick up one side of the graphene flake and fold it over to the other half, forming t-BLG.[125] However, this method relies heavily on the availability of the instrument and the experience of the human operator.

Category 3. Another category of moiré superlattices involves inducing a nanoscale periodic potential within the 2D material channel through nanolithography patterning of either the dielectric substrates[126,127] or the gate electrode[128] (see Figure 9d). By replacing the nuanced process of creating small-angle rotation with standard nanofabrication of patterned dielectrics or electrodes, this strategy considerably improves the reproducibility and yield of the fabrication process. Moreover, it enriches the kinds of lattice symmetries to more than triangular moiré superlattices.[126]

7.2. Disorders in Moiré Materials

The fabrication process for moiré superlattices largely follows the same procedures outlined in Sections 1–3 for constructing simple heterostructures. Therefore, similar material disorders, such as intrinsic defects or extrinsic interfacial residues, are expected to appear in moiré materials. Achieving atomically clean interfaces is essential for moiré superlattices because it promotes coherent carrier transport and facilitates strong interlayer coupling, both of which are vital for the emergence of correlated states linked to moiré physics. Experimental evidence has demonstrated the crucial role of interlayer coupling in revealing and enhancing moiré physics. This was achieved by applying external pressure as a means to adjust the extent of the coupling.[129,130]

Furthermore, apart from the above-mentioned material disorders, moiré materials are also affected by additional structural irregularities. Due to the inverse relationship between moiré wavelength and lattice mismatch (δ) or twist angle (θ), minor fluctuations in strain and rotation can be magnified in moiré superlattices. In the following discussion, we focus on these structural irregularities and explore research efforts aimed at mitigating their impact.

Strain variations can directly affect the local electronic band structure by altering the size of the superlattice unit cell[131,132] (see Figure 9e). In heterobilayer superlattices, the moiré band structure is determined by the lattice mismatch between the two constituent layers, making these structures highly vulnerable to strain variations. In homobilayers, strain variations may arise during the process of tearing a single graphene flake. To mitigate strain fluctuations resulting from tearing, the flake can be pre-cut using a laser[124,133] or an AFM tip.[134] Additionally, other sources of strain disorder may occur during the layer transfer and metallization steps.

The spatial inhomogeneity of twist angle in homobilayers persists as a prevalent disorder in existing fabrication techniques. This issue is particularly pronounced in small-angle moiré systems, which typically remain in a metastable state, resulting in fluctuations in the measured charge density (see Figure 9f).[135–138] Furthermore, during the fabrication process, small-angle rotations on the order of a few degrees in t-BLG tend to relax to a Bernal stack configuration, as it represents the thermodynamically stable state.[120] This challenge significantly contributes to the low yield in constructing homobilayer twistronics. Since the angle relaxation occurs toward the thermodynamically stable state, the resulting homobilayers have smaller twist angle than their initially twisted value. Therefore, a possible solution has been to account for this angle relaxation when implementing the tear-and-stack step.

Domain reconstruction also contributes to the inhomogeneity in moiré superlattices with twist angles smaller than the critical value ≈1°, where heterostructures tend to maximize the area of AB stacking instead of AA stacking, forming alternating domains of AB/BA areas (see Figure 9g).[139,140]

The above-mentioned issues associated with angle disorders are less significant in heterobilayers because they naturally align at angles that are thermodynamically stable. Therefore, to address small-angle misalignments in heterobilayers, a common practice is to perform thermal annealing, allowing the superlattices to relax back to aligned angles[32,120,141] (see Figure 9h). In contrast and considering the metastability of homobilayers, it is therefore essential to avoid high-temperature processing steps during their construction, such as thermal annealing for interface cleaning, or even resist baking for lithography.

8. Outlook

The success of the vdW stacking method in achieving ultralow disordered BGB heterostructures has occurred by avoiding contaminations, such as polymers, organic solvents, and water during the fabrication process. Over the years, research laboratories have independently developed material production, cleaning, and assembly protocols under the guidelines of minimizing exposure to contaminants. To further improve the fabrication process, the material exfoliation and layer assembly processes were also performed in controlled environments, such as a glovebox or a vacuum chamber. Despite these advances, scaling up the dimensions and fabrication throughputs of ultralow disordered heterostructures using the vdW stacking method remains challenging.

We presented recent advances in developing new engineering toolkits for enhancing the outcomes of the exfoliation in terms of dimension and production throughput. However, these advances come with a trade-off: increased exposure to contaminants. This drawback presents a challenge for creating ultralow disordered heterostructures. This discussion leads to a fundamental question: Can contaminated 2D layers achieve ultralow disordered heterostructures on par with their state-of-the-art counterparts?

The short answer is "Yes." Nevertheless, the types of contaminants and the details of the fabrication process will determine the ultimate outcome. A survey of previous research showed that exposure to PMMA polymer, for instance, can result in an irreversible contamination of graphene. Moreover, the direct evaporation of metals onto 2D layers has been shown to create additional atomic defects. In contrast, PVA-contaminated graphene has been successfully utilized in achieving record large-area BGB heterostructures with state-of-the-art electronic transport properties. The full removal of interfacial contaminants in these BGB structures represents an encouraging advance, opening several new research directions.

The first is performing computational studies to reveal the nature of interactions between various contaminants and a target 2D flake. For instance, the current studies on PMMA, PVA, and small organic molecules were instrumental in guiding the interface cleaning studies of the contaminated heterostructures. The desired contaminants are those that would interact non-covalently with the 2D flakes, allowing the possibility for their removal from the heterostructure through an interface cleaning approach.

This brings us to the second research direction, which involves the discovery of new polymers that can serve as handle layers while facilitating the interface cleaning process. In the case of PVA, it was found that mobilization of residues occurred only at elevated temperatures (230 °C), coinciding with an increased entropy of the PVA due to a phase transition.[142] Building on the success of PVA as a model polymer, we pose a question: Can a new polymer be designed that retains the desirable properties of PVA (e.g., enhanced exfoliation) while allowing the mobilization of residues at significantly lower temperatures?

Stamp engineering has proven to be a powerful engineering toolkit. Building on those advances, the third direction involves the design of new stamp geometry. Recent studies have shown that the deformation energy and contact angle of the stamp play a key role in the interface cleaning of polymer-contaminated heterostructures.[56] However, computational studies are still lacking, linking the geometric properties of the stamp and the dynamics of the layer transfer process to the elastic energy and evolution of the contact angle at the lamination front. Conducting such studies will provide valuable insights into advancing the interface cleaning process.

The carrier transport results from the BGB heterostructures made from polymer-contaminated graphene are highly promising.[56] However, high carrier mobility alone is insufficient to establish that the heterostructures obtained from emerging engineering toolkits are low disorder. Detailed quantum transport measurements are necessary to reveal the underlying scattering mechanisms in those heterostructures. These results will allow a comprehensive comparison with state-of-the-art counterparts fabricated using the vdW stacking method. Moreover, the strong interlayer coupling to form moiré superlattices is yet another compelling evidence for the ability of emerging engineering toolkits to create ultralow disordered electronic systems. These experiments constitute the fourth research direction.

Fabrication of moiré materials presents additional research challenges, detracting from the reproducibility and homogeneity of the superlattice heterostructures. In particular, angle and strain disorders induce microscopic variations in the electronic band structure within the same superlattice heterostructure. Therefore, there is a critical research need to develop fabrication techniques, such as improved alignment techniques, or innovative handling and transfer methods, that ensure homogeneous interfaces without contamination, along with minimal strain and angle disorders.

A final and crucial research direction is to establish manufacturing pathways for production of ultralow disordered heterostructures, which encompasses two main aspects. One is the need for wafer-scale fabrication processing of 2D materials. The other aspect involves the fully automated fabrication process of these heterostructures.

The current prevalence of the exfoliated flakes for producing ultralow disordered heterostructures is due to their inherently low intrinsic disorders. However, the existing parent crystals used for mechanical exfoliation are typically millimeter-scale, making them unsuitable for wafer-scale manufacturing of such heterostructures. To develop manufacturable pathways and facilitate the technological translation of ultralow disordered heterostructures, fabrication methods based on large-area synthetic materials like CVD films remain a crucial research direction. Advances in various aspects of CVD materials have been made, including the production of wafer-scale single-crystal CVD films (e.g., Ref. [143]) and layer assembly (e.g., Ref. [144]) merits a comprehensive review of the significant advances in this domain. We emphasize, however, that many aspects of the emerging engineering toolkits discussed in this article, such as cleaning of interfaces within heterostructures, fabrication of low disordered moiré superlattices, and production of heterostructures from air-sensitive 2D materials, are applicable to CVD materials.

The current practice for fabricating vdW heterostructure heavily relies on the manual layer assembly setup. The reliability and reproducibility of building high-quality heterostructures depends on the expertise of the human operator. Recent efforts have been made to build a programmed stacker for streamlining the production of vdW heterostructures.[145,146] A recent study demonstrated an automatic process for searching and assembling exfoliated 2D flakes in a glovebox environment.[145] Fabricating vdW heterostructures using a robotic operator can ensure consistent process parameters, thereby improving the reproducibility of heterostructure construction. Moreover, to achieve accurate control over small rotation while fabricating moiré materials, it is more reliable to employ a motorized stage.

Lastly, it is important to emphasize that a fundamental understanding of various engineering toolkits is essential for their successful translation into an automated process. Enabling the nanomanufacturing of vdW heterostructures will require collaboration efforts across various disciplines, including materials science, chemistry, and physics. We anticipate that a fully automated fabrication process will not only accelerate scientific discoveries but also facilitate their subsequent translation into technological applications.

Acknowledgements

D.S. acknowledges support from NSF award #2 224 139.

Conflict of Interest

The authors declare no conflict of interest.

Keywords

interface cleaning, graphene, heterostructure, moire superlattice, van der Waals

Received: November 16, 2023
Revised: April 13, 2024
Published online: June 3, 2024

[1] Y. Kim, A. C. Balram, T. Taniguchi, K. Watanabe, J. K. Jain, J. H. Smet, *Nat. Phys.* **2019**, *15*, 154.
[2] K. Komatsu, Y. Morita, E. Watanabe, D. Tsuya, K. Watanabe, T. Taniguchi, S. Moriyama, *Sci. Adv.* **2018**, *4*, eaaq0194.
[3] C. R. Dean, L. Wang, P. Maher, C. Forsythe, F. Ghahari, Y. Gao, J. Katoch, M. Ishigami, P. Moon, M. Koshino, T. Taniguchi, K. Watanabe, K. L. Shepard, J. Hone, P. Kim, *Nature* **2013**, *497*, 598.
[4] B. Hunt, J. D. Sanchez-Yamagishi, A. F. Young, M. Yankowitz, B. J. LeRoy, K. Watanabe, T. Taniguchi, P. Moon, M. Koshino, P. Jarillo-Herrero, R. C. Ashoori, *Science* **2013**, *340*, 1427.
[5] X. Sun, S. Zhang, Z. Liu, H. Zhu, J. Huang, K. Yuan, Z. Wang, K. Watanabe, T. Taniguchi, X. Li, M. Zhu, J. Mao, T. Yang, J. Kang, J. Liu, Y. Ye, Z. V. Han, Z. Zhang, *Nat. Commun.* **2021**, *12*, 7196.
[6] Y. Zeng, J. I. A. Li, S. A. Dietrich, O. M. Ghosh, K. Watanabe, T. Taniguchi, J. Hone, C. R. Dean, *Phys. Rev. Lett.* **2019**, *122*, 137701.
[7] L. Wang, S. Zihlmann, M.-H. Liu, P. Makk, K. Watanabe, T. Taniguchi, A. Baumgartner, C. Schönenberger, *Nano Lett.* **2019**, *19*, 2371.
[8] X. Cui, G.-H. Lee, Y. D. Kim, G. Arefe, P. Y. Huang, C.-H. Lee, D. A. Chenet, X. Zhang, L. Wang, F. Ye, F. Pizzocchero, B. S. Jessen, K. Watanabe, T. Taniguchi, D. A. Muller, T. Low, P. Kim, J. Hone, *Nat. Nanotechnol.* **2015**, *10*, 534.
[9] C. Déprez, L. Veyrat, H. Vignaud, G. Nayak, K. Watanabe, T. Taniguchi, F. Gay, H. Sellier, B. Sacépé, *Nat. Nanotechnol.* **2021**, *16*, 555.
[10] L. Veyrat, C. Déprez, A. Coissard, X. Li, F. Gay, K. Watanabe, T. Taniguchi, Z. Han, B. A. Piot, H. Sellier, B. Sacépé, *Science* **2020**, *367*, 781.
[11] A. Castellanos-Gomez, X. Duan, Z. Fei, H. R. Gutierrez, Y. Huang, X. Huang, J. Quereda, Q. Qian, E. Sutter, P. Sutter, *Nature Reviews Methods Primers* **2022**, *2*, 58.
[12] A. K. Geim, I. V. Grigorieva, *Nature* **2013**, *499*, 419.
[13] K. S. Novoselov, A. Mishchenko, A. Carvalho, A. H. Castro Neto, *Science* **2016**, *353*, aac9439.
[14] L. Sun, G. Yuan, L. Gao, J. Yang, M. Chhowalla, M. H. Gharahcheshmeh, K. K. Gleason, Y. S. Choi, B. H. Hong, Z. Liu, *Nature Reviews Methods Primers* **2021**, *1*, 5.
[15] S. Fan, Q. A. Vu, M. D. Tran, S. Adhikari, Y. H. Lee, *2D Mater.* **2020**, *7*, 022005.
[16] R. Frisenda, E. Navarro-Moratalla, P. Gant, D. Pérez De Lara, P. Jarillo-Herrero, R. V. Gorbachev, A. Castellanos-Gomez, *Chem. Soc. Rev.* **2018**, *47*, 53.
[17] M. Onodera, S. Masubuchi, R. Moriya, T. Machida, *Jpn. J. Appl. Phys.* **2020**, *59*, 010101.
[18] H.-Z. Zhang, W.-J. Wu, L. Zhou, Z. Wu, J. Zhu, *Small Science* **2022**, *2*, 2100033.
[19] S. H. Choi, S. J. Yun, Y. S. Won, C. S. Oh, S. M. Kim, K. K. Kim, Y. H. Lee, *Nat. Commun.* **2022**, *13*, 1484.
[20] J. C. Song, N. M. Gabor, *Nat. Nanotechnol.* **2018**, *13*, 986.
[21] M. Yankowitz, Q. Ma, P. Jarillo-Herrero, B. J. LeRoy, *Nature Reviews Physics* **2019**, *1*, 112.
[22] C. N. Lau, M. W. Bockrath, K. F. Mak, F. Zhang, *Nature* **2022**, *602*, 41.
[23] A. Ciarrocchi, F. Tagarelli, A. Avsar, A. Kis, *Nat. Rev. Mater.* **2022**, *7*, 449.
[24] Y. Liu, Y. Huang, X. Duan, *Nature* **2019**, *567*, 323.
[25] C. Liu, H. Chen, S. Wang, Q. Liu, Y.-G. Jiang, D. W. Zhang, M. Liu, P. Zhou, *Nat. Nanotechnol.* **2020**, *15*, 545.
[26] S. Das, A. Sebastian, E. Pop, C. J. McClellan, A. D. Franklin, T. Grasser, T. Knobloch, Y. Illarionov, A. V. Penumatcha, J. Appenzeller, Z. Chen, W. Zhu, I. Asselberghs, L.-J. Li, U. E. Avci, N. Bhat, T. D. Anthopoulos, R. Singh, *Nat. Electron.* **2021**, *4*, 786.
[27] M. C. Lemme, D. Akinwande, C. Huyghebaert, C. Stampfer, *Nat. Commun.* **2022**, *13*, 1392.
[28] T. Knobloch, Y. Y. Illarionov, F. Ducry, C. Schleich, S. Wachter, K. Watanabe, T. Taniguchi, T. Mueller, M. Waltl, M. Lanza, M. I. Vexler, M. Luisier, T. Grasser, *Nat. Electron.* **2021**, *4*, 98.
[29] D. Rhodes, S. H. Chae, R. Ribeiro-Palau, J. Hone, *Nat. Mater.* **2019**, *18*, 541.
[30] C. R. Dean, A. F. Young, I. Meric, C. Lee, L. Wang, S. Sorgenfrei, K. Watanabe, T. Taniguchi, P. Kim, K. L. Shepard, J. Hone, *Nat. Nanotechnol.* **2010**, *5*, 722.
[31] L. Wang, I. Meric, P. Y. Huang, Q. Gao, Y. Gao, H. Tran, T. Taniguchi, K. Watanabe, L. M. Campos, D. A. Muller, J. Guo, P. Kim, J. Hone, K. L. Shepard, C. R. Dean, *Science* **2013**, *342*, 614.
[32] L. Wang, Y. Gao, B. Wen, Z. Han, T. Taniguchi, K. Watanabe, M. Koshino, J. Hone, C. R. Dean, *Science* **2015**, *350*, 1231.
[33] D. A. Sanchez, Z. Dai, P. Wang, A. Cantu-Chavez, C. J. Brennan, R. Huang, N. Lu, *Proc. Natl. Acad. Sci. USA* **2018**, *115*, 7884.
[34] A. V. Kretinin, Y. Cao, J. S. Tu, G. L. Yu, R. Jalil, K. S. Novoselov, S. J. Haigh, A. Gholinia, A. Mishchenko, M. Lozada, T. Georgiou, C. R. Woods, F. Withers, P. Blake, G. Eda, A. Wirsig, C. Hucho, K. Watanabe, T. Taniguchi, A. K. Geim, R. V. Gorbachev, *Nano Lett.* **2014**, *14*, 3270.
[35] F. Liu, W. Wu, Y. Bai, S. H. Chae, Q. Li, J. Wang, J. Hone, X.-Y. Zhu, *Science* **2020**, *367*, 903.
[36] S. B. Desai, S. R. Madhvapathy, M. Amani, D. Kiriya, M. Hettick, M. Tosun, Y. Zhou, M. Dubey, J. W. Ager, D. Chrzan, A. Javey, *Adv. Mater.* **2016**, *28*, 4053.
[37] J.-Y. Moon, M. Kim, S.-I. Kim, S. Xu, J.-H. Choi, D. Whang, K. Watanabe, T. Taniguchi, D. S. Park, J.-H. Lee, *Sci. Adv.* **2020**, *6*, eabc6601.
[38] Y. Huang, Y.-H. Pan, R. Yang, L.-H. Bao, L. Meng, H.-L. Luo, Y.-Q. Cai, G.-D. Liu, W.-J. Zhao, Z. Zhou, L.-M. Wu, Z.-L. Zhu, M. Huang, L.-W. Liu, L. Liu, P. Cheng, K.-H. Wu, S.-B. Tian, C.-Z. Gu, Y.-G. Shi, Y.-F. Guo, Z. G. Cheng, J.-P. Hu, L. Zhao, G.-H. Yang, E. Sutter, P. Sutter, Y.-L. Wang, W. Ji, X.-J. Zhou, et al., *Nat. Commun.* **2020**, *11*, 2453.
[39] J. Shim, S.-H. Bae, W. Kong, D. Lee, K. Qiao, D. Nezich, Y. J. Park, R. Zhao, S. Sundaram, X. Li, H. Yeon, C. Choi, H. Kum, R. Yue, G. Zhou, Y. Ou, K. Lee, J. Moodera, X. Zhao, J.-H. Ahn, C. Hinkle, A. Ougazzaden, J. Kim, *Science* **2018**, *362*, 665.
[40] J. Kim, H. Park, J. B. Hannon, S. W. Bedell, K. Fogel, D. K. Sadana, C. Dimitrakopoulos, *Science* **2013**, *342*, 833.
[41] Y. Liu, J. Guo, E. Zhu, L. Liao, S.-J. Lee, M. Ding, I. Shakir, V. Gambin, Y. Huang, X. Duan, *Nature* **2018**, *557*, 696.
[42] Y. Jung, M. S. Choi, A. Nipane, A. Borah, B. Kim, A. Zangiabadi, T. Taniguchi, K. Watanabe, W. J. Yoo, J. Hone, J. T. Teherani, *Nat. Electron.* **2019**, *2*, 187.
[43] Y. Huang, E. Sutter, N. N. Shi, J. Zheng, T. Yang, D. Englund, H.-J. Gao, P. Sutter, *ACS Nano* **2015**, *9*, 10612.
[44] P. Pedrinazzi, J. M. Caridad, D. M. A. Mackenzie, F. Pizzocchero, L. Gammelgaard, B. S. Jessen, R. Sordan, T. J. Booth, P. Bøggild, *Appl. Phys. Lett.* **2018**, *112*, 33101.
[45] K. Kinoshita, R. Moriya, M. Onodera, Y. Wakafuji, S. Masubuchi, K. Watanabe, T. Taniguchi, T. Machida, *npj 2D Materials and Applications* **2019**, *3*, 22.
[46] P. Blake, E. W. Hill, A. H. Castro Neto, K. S. Novoselov, D. Jiang, R. Yang, T. J. Booth, A. K. Geim, *Appl. Phys. Lett.* **2007**, *91*, 63124.
[47] Z. Huang, A. Alharbi, W. Mayer, E. Cuniberto, T. Taniguchi, K. Watanabe, J. Shabani, D. Shahrjerdi, *Nat. Commun.* **2020**, *11*, 3029.
[48] J. S. Park, J. W. Park, E. Ruckenstein, *Journal of applied polymer science* **2001**, *82*, 1816.
[49] F. Pizzocchero, L. Gammelgaard, B. S. Jessen, J. M. Caridad, L. Wang, J. Hone, P. Bøggild, T. J. Booth, *Nat. Commun.* **2016**, *7*, 11894.
[50] P. J. Zomer, M. H. D. Guimarães, J. C. Brant, N. Tombros, B. J. van Wees, *Appl. Phys. Lett.* **2014**, *105*, 013101.

[51] A. Castellanos-Gomez, M. Buscema, R. Molenaar, V. Singh, L. Janssen, H. S. J. van der Zant, G. A. Steele, *2D Mater.* **2014**, *1*, 011002.
[52] S. Kim, J. Wu, A. Carlson, S. H. Jin, A. Kovalsky, P. Glass, Z. Liu, N. Ahmed, S. L. Elgan, W. Chen, P. M. Ferreira, M. Sitti, Y. Huang, J. A. Rogers, *Proc. Natl. Acad. Sci. USA* **2010**, *107*, 17095.
[53] M. A. Meitl, Z.-T. Zhu, V. Kumar, K. J. Lee, X. Feng, Y. Y. Huang, I. Adesida, R. G. Nuzzo, J. A. Rogers, *Nat. Mater.* **2006**, *5*, 33.
[54] K. Kim, M. Yankowitz, B. Fallahazad, S. Kang, H. C. P. Movva, S. Huang, S. Larentis, C. M. Corbet, T. Taniguchi, K. Watanabe, S. K. Banerjee, B. J. LeRoy, E. Tutuc, *Nano Lett.* **2016**, *16*, 1989.
[55] S. Toyoda, T. Uwanno, T. Taniguchi, K. Watanabe, K. Nagashio, *Appl. Phys. Express* **2019**, *12*, 055008.
[56] Z. Huang, E. Cuniberto, S. Park, K. Kisslinger, Q. Wu, T. Taniguchi, K. Watanabe, K. G. Yager, D. Shahrjerdi, *Small* **2022**, *18*, 2201248.
[57] D. G. Purdie, N. M. Pugno, T. Taniguchi, K. Watanabe, A. C. Ferrari, A. Lombardo, *Nat. Commun.* **2018**, *9*, 5387.
[58] T. Iwasaki, K. Endo, E. Watanabe, D. Tsuya, Y. Morita, S. Nakaharai, Y. Noguchi, Y. Wakayama, K. Watanabe, T. Taniguchi, S. Moriyama, *ACS Appl. Mater. Interfaces* **2020**, *12*, 8533.
[59] F. Joucken, C. Bena, Z. Ge, E. Quezada-Lopez, S. Pinon, V. Kaladzhyan, T. Taniguchi, K. Watanabe, A. Ferreira, J. Velasco, *Nano Lett.* **2021**, *21*, 7100.
[60] D. Wong, J. Velasco, L. Ju, J. Lee, S. Kahn, H.-Z. Tsai, C. Germany, T. Taniguchi, K. Watanabe, A. Zettl, F. Wang, M. F. Crommie, *Nat. Nanotechnol.* **2015**, *10*, 949.
[61] J. Hong, Z. Hu, M. Probert, K. Li, D. Lv, X. Yang, L. Gu, N. Mao, Q. Feng, L. Xie, J. Zhang, D. Wu, Z. Zhang, C. Jin, W. Ji, X. Zhang, J. Yuan, Z. Zhang, *Nat. Commun.* **2015**, *6*, 6293.
[62] A. Jain, P. Bharadwaj, S. Heeg, M. Parzefall, T. Taniguchi, K. Watanabe, L. Novotny, *Nanotechnology* **2018**, *29*, 265203.
[63] H. Ghorbanfekr-Kalashami, K. S. Vasu, R. R. Nair, F. M. Peeters, M. Neek-Amal, *Nat. Commun.* **2017**, *8*, 15844.
[64] B. H. Tan, J. Zhang, J. Jin, C. Hong Ooi, Y. He, R. Zhou, K. Ostrikov, N.-T. Nguyen, H. An, *Nano Lett.* **2020**, *20*, 3478.
[65] E. Khestanova, F. Guinea, L. Fumagalli, A. K. Geim, I. V. Grigorieva, *Nat. Commun.* **2016**, *7*, 12587.
[66] Z. Dai, Y. Hou, D. A. Sanchez, G. Wang, C. J. Brennan, Z. Zhang, L. Liu, N. Lu, *Phys. Rev. Lett.* **2018**, *121*, 266101.
[67] C. Ma, Y. Chen, J. Chu, *Langmuir* **2023**, *39*, 701.
[68] C. Ma, Y. Chen, J. Chu, *Langmuir* **2023**, *39*, 709.
[69] P. Cao, K. Xu, J. O. Varghese, J. R. Heath, *Nano Lett.* **2011**, *11*, 5581.
[70] P. Schweizer, C. Dolle, D. Dasler, G. Abellán, F. Hauke, A. Hirsch, E. Spiecker, *Nat. Commun.* **2020**, *11*, 1743.
[71] S. J. Haigh, A. Gholinia, R. Jalil, S. Romani, L. Britnell, D. C. Elias, K. S. Novoselov, L. A. Ponomarenko, A. K. Geim, R. Gorbachev, *Nat. Mater.* **2012**, *11*, 764.
[72] P. Lazar, F. Karlický, P. Jurecka, M. Kocman, E. Otyepková, K. Safárová, M. Otyepka, *J. Am. Chem. Soc.* **2013**, *135*, 6372.
[73] Y.-C. Lin, C.-C. Lu, C.-H. Yeh, C. Jin, K. Suenaga, P.-W. Chiu, *Nano Lett.* **2012**, *12*, 414.
[74] W. S. Leong, H. Wang, J. Yeo, F. J. Martin-Martinez, A. Zubair, P.-C. Shen, Y. Mao, T. Palacios, M. J. Buehler, J.-Y. Hong, J. Kong, *Nat. Commun.* **2019**, *10*, 867.
[75] A. G. F. Garcia, M. Neumann, F. Amet, J. R. Williams, K. Watanabe, T. Taniguchi, D. Goldhaber-Gordon, *Nano Lett.* **2012**, *12*, 4449.
[76] F. Amet, A. J. Bestwick, J. R. Williams, L. Balicas, K. Watanabe, T. Taniguchi, D. Goldhaber-Gordon, *Nat. Commun.* **2015**, *6*, 583.
[77] M. Yankowitz, S. Larentis, K. Kim, J. Xue, D. McKenzie, S. Huang, M. Paggen, M. N. Ali, R. J. Cava, E. Tutuc, B. J. LeRoy, *Nano Lett.* **2015**, *15*, 1925.
[78] J. Katoch, S. Ulstrup, R. J. Koch, S. Moser, K. M. McCreary, S. Singh, J. Xu, B. T. Jonker, R. K. Kawakami, A. Bostwick, E. Rotenberg, C. Jozwiak, *Nat. Phys.* **2018**, *14*, 355.
[79] M. Tripathi, A. Mittelberger, K. Mustonen, C. Mangler, J. Kotakoski, J. C. Meyer, T. Susi, *physica status solidi (RRL)–Rapid Research Letters* **2017**, *11*, 1700124.
[80] B. Zhuang, S. Li, S. Li, J. Yin, *Carbon* **2021**, *173*, 609.
[81] Y. Kim, P. Herlinger, T. Taniguchi, K. Watanabe, J. H. Smet, *ACS Nano* **2019**, *13*, 14182.
[82] M. R. Rosenberger, H. J. Chuang, K. M. McCreary, A. T. Hanbicki, S. V. Sivaram, B. T. Jonker, *ACS Appl. Mater. Interfaces* **2018**, *10*, 10379.
[83] H. W. Guo, Z. Hu, Z. B. Liu, J. G. Tian, *Adv. Funct. Mater.* **2021**, *31*, 2007810.
[84] A. P. Rooney, A. Kozikov, A. N. Rudenko, E. Prestat, M. J. Hamer, F. Withers, Y. Cao, K. S. Novoselov, M. I. Katsnelson, R. Gorbachev, S. J. Haigh, *Nano Lett.* **2017**, *17*, 5222.
[85] S. Guo, M. Luo, G. Shi, N. Tian, Z. Huang, F. Yang, L. Ma, N. Z. Wang, Q. Shi, K. Xu, Z. Xu, K. Watanabe, T. Taniguchi, X. H. Chen, D. Shen, L. Zhang, W. Ruan, Y. Zhang, *Rev. Sci. Instrum.* **2023**, *94*, 13903.
[86] W. Wang, N. Clark, M. Hamer, A. Carl, E. Tovari, S. Sullivan-Allsop, E. Tillotson, Y. Gao, H. de Latour, F. Selles, J. Howarth, E. G. Castanon, M. Zhou, H. Bai, X. Li, A. Weston, K. Watanabe, T. Taniguchi, C. Mattevi, T. H. Bointon, P. V. Wiper, A. J. Strudwick, L. A. Ponomarenko, A. V. Kretinin, S. J. Haigh, A. Summerfield, R. Gorbachev, *Nat. Electron.* **2023**, *6*, 981.
[87] A. Favron, E. Gaufrès, F. Fossard, A.-L. Phaneuf-L'Heureux, N. Y.-W. Tang, P. L. Lévesque, A. Loiseau, R. Leonelli, S. Francoeur, R. Martel, *Nat. Mater.* **2015**, *14*, 826.
[88] J. Pei, X. Gai, J. Yang, X. Wang, Z. Yu, D.-Y. Choi, B. Luther-Davies, Y. Lu, *Nat. Commun.* **2016**, *7*, 10450.
[89] Y. Cao, A. Mishchenko, G. L. Yu, E. Khestanova, A. P. Rooney, E. Prestat, A. V. Kretinin, P. Blake, M. B. Shalom, C. Woods, J. Chapman, G. Balakrishnan, I. V. Grigorieva, K. S. Novoselov, B. A. Piot, M. Potemski, K. Watanabe, T. Taniguchi, S. J. Haigh, A. K. Geim, R. V. Gorbachev, *Nano Lett.* **2015**, *15*, 4914.
[90] Z. Xu, W. Chen, J. Huang, W. Tian, S. Chen, W. Yue, T. Chi, Y. Y. Lyu, H. Sun, Y. L. Wang, G. Sun, *Appl. Phys. Lett.* **2021**, *119*, 072601.
[91] G.-H. Lee, S. Kim, S.-H. Jhi, H.-J. Lee, *Nat. Commun.* **2015**, *6*, 6181.
[92] M. Kim, G.-H. Park, J. Lee, J. H. Lee, J. Park, H. Lee, G.-H. Lee, H.-J. Lee, *Nano Lett.* **2017**, *17*, 6125.
[93] J. Cai, E. Anderson, C. Wang, X. Zhang, X. Liu, W. Holtzmann, Y. Zhang, F. Fan, T. Taniguchi, K. Watanabe, Y. Ran, T. Cao, L. Fu, D. Xiao, W. Yao, X. Xu, *Nature* **2023**, *622*, 63.
[94] Y. Deng, X. Zhao, C. Zhu, P. Li, R. Duan, G. Liu, Z. Liu, *ACS Nano* **2021**, *15*, 12465.
[95] H. Park, J. Cai, E. Anderson, Y. Zhang, J. Zhu, X. Liu, C. Wang, W. Holtzmann, C. Hu, Z. Liu, T. Taniguchi, K. Watanabe, J.-H. Chu, T. Cao, L. Fu, W. Yao, C.-Z. Chang, D. Cobden, D. Xiao, X. Xu, *Nature* **2023**, *622*, 74.
[96] A. N. Hoffman, M. G. Stanford, C. Zhang, I. N. Ivanov, A. D. Oyedele, M. G. Sales, S. J. McDonnell, M. R. Koehler, D. G. Mandrus, L. Liang, B. G. Sumpter, *ACS Appl. Mater. Interfaces* **2018**, *10*, 36540.
[97] F. Ye, J. Lee, J. Hu, Z. Mao, J. Wei, P. X. L. Feng, *Small* **2016**, *12*, 5802.
[98] H. Zhu, Q. Wang, L. Cheng, R. Addou, J. Kim, M. J. Kim, R. M. Wallace, *ACS Nano* **2017**, *11*, 11005.
[99] Q. Li, Q. Zhou, L. Shi, Q. Chen, J. Wang, *J. Mater. Chem. A* **2019**, *7*, 4291.
[100] G. Mirabelli, C. McGeough, M. Schmidt, E. K. McCarthy, S. Monaghan, I. M. Povey, M. McCarthy, F. Gity, R. Nagle, G. Hughes, A. Cafolla, P. K. Hurley, R. Duffy, *J. Appl. Phys.* **2016**, *120*, 125102.
[101] M. van Druenen, *Adv. Mater. Interfaces* **2020**, *7*, 2001102.
[102] Y. Huang, J. Qiao, K. He, S. Bliznakov, E. Sutter, X. Chen, D. Luo, F. Meng, D. Su, J. Decker, W. Ji, R. S. Ruoff, P. Sutter, *Chem. Mater.* **2016**, *28*, 8330.

[103] D. A. Bandurin, A. V. Tyurnina, G. L. Yu, A. Mishchenko, V. Zólyomi, S. V. Morozov, R. K. Kumar, R. V. Gorbachev, Z. R. Kudrynskyi, S. Pezzini, Z. D. Kovalyuk, U. Zeitler, K. S. Novoselov, A. Patanè, L. Eaves, I. V. Grigorieva, V. I. Fal'ko, A. K. Geim, Y. Cao, *Nat. Nanotechnol.* **2017**, *12*, 223.
[104] X. Chen, Z. Yang, S. Feng, T. W. Golbek, W. Xu, H.-J. Butt, T. Weidner, Z. Xu, J. Hao, Z. Wang, *Nano Lett.* **2020**, *20*, 5670.
[105] Q. Yan, Y. Weng, S. Wang, Z. Zhou, Y. Hu, Q. Li, J. Xue, Z. Feng, Z. Luo, R. Feng, L. You, *ACS Appl. Mater. Interfaces* **2024**, *16*, 9051.
[106] N. Clark, L. Nguyen, M. J. Hamer, F. Schedin, E. A. Lewis, E. Prestat, A. Garner, Y. Cao, M. Zhu, R. Kashtiban, J. Sloan, D. Kepaptsoglou, R. V. Gorbachev, S. J. Haigh, *Nano Lett.* **2018**, *18*, 5373.
[107] V. Tayari, N. Hemsworth, I. Fakih, A. Favron, E. Gaufrès, G. Gervais, R. Martel, T. Szkopek, *Nat. Commun.* **2015**, *6*, 7702.
[108] L. Lanoël, G. Rozas, A. E. Bruchhausen, M. L. Amigó, M. V. A. Crivillero, J. A. Hofer, M. Villafuerte, G. Bridoux, S. Bengió, G. Nieva, *Phys. Rev. B* **2022**, *106*, 214507.
[109] M. T. Edmonds, A. Tadich, A. Carvalho, A. Ziletti, K. M. O'Donnell, S. P. Koenig, D. F. Coker, B. Ozyilmaz, A. C. Neto, M. S. Fuhrer, *ACS Appl. Mater. Interfaces* **2015**, *7*, 14557.
[110] M. Yankowitz, J. Xue, D. Cormode, J. D. Sanchez-Yamagishi, K. Watanabe, T. Taniguchi, P. Jarillo-Herrero, P. Jacquod, B. J. LeRoy, *Nat. Phys.* **2012**, *8*, 382.
[111] G. Chen, A. L. Sharpe, P. Gallagher, I. T. Rosen, E. J. Fox, L. Jiang, B. Lyu, H. Li, K. Watanabe, T. Taniguchi, J. Jung, Z. Shi, D. Goldhaber-Gordon, Y. Zhang, F. Wang, *Nature* **2019**, *572*, 215.
[112] H. Zhou, T. Xie, A. Ghazaryan, T. Holder, J. R. Ehrets, E. M. Spanton, T. Taniguchi, K. Watanabe, E. Berg, M. Serbyn, A. F. Young, *Nature* **2021**, *598*, 429.
[113] H. Zhou, T. Xie, T. Taniguchi, K. Watanabe, A. F. Young, *Nature* **2021**, *598*, 434.
[114] K. Kim, V. I. Artyukhov, W. Regan, Y. Liu, M. F. Crommie, B. I. Yakobson, A. Zettl, *Nano Lett.* **2012**, *12*, 293.
[115] Y. Guo, C. Liu, Q. Yin, C. Wei, S. Lin, T. B. Hoffman, Y. Zhao, J. H. Edgar, Q. Chen, S. P. Lau, J. Dai, H. Yao, H.-S. P. Wong, Y. Chai, *ACS Nano* **2016**, *10*, 8980.
[116] Y. Li, Y. Rao, K. F. Mak, Y. You, S. Wang, C. R. Dean, T. F. Heinz, *Nano Lett.* **2013**, *13*, 3329.
[117] N. Kumar, S. Najmaei, Q. Cui, F. Ceballos, P. M. Ajayan, J. Lou, H. Zhao, *Phys. Rev. B* **2013**, *87*, 161403.
[118] E. C. Regan, D. Wang, C. Jin, M. I. Bakti Utama, B. Gao, X. Wei, S. Zhao, W. Zhao, Z. Zhang, K. Yumigeta, M. Blei, J. D. Carlström, K. Watanabe, T. Taniguchi, S. Tongay, M. Crommie, A. Zettl, F. Wang, *Nature* **2020**, *579*, 359.
[119] C. Casiraghi, A. Hartschuh, H. Qian, S. Piscanec, C. Georgi, A. Fasoli, K. S. Novoselov, D. M. Basko, A. C. Ferrari, *Nano Lett.* **2009**, *9*, 1433.
[120] C. R. Woods, F. Withers, M. J. Zhu, Y. Cao, G. Yu, A. Kozikov, M. Ben Shalom, S. V. Morozov, M. M. van Wijk, A. Fasolino, M. I. Katsnelson, K. Watanabe, T. Taniguchi, A. K. Geim, A. Mishchenko, K. S. Novoselov, *Nat. Commun.* **2016**, *7*, 10800.
[121] F. Fabbri, E. Rotunno, E. Cinquanta, D. Campi, E. Bonnini, D. Kaplan, L. Lazzarini, M. Bernasconi, C. Ferrari, M. Longo, G. Nicotra, A. Molle, V. Swaminathan, G. Salviati, *Nat. Commun.* **2016**, *7*, 13044.
[122] Y. Cao, V. Fatemi, A. Demir, S. Fang, S. L. Tomarken, J. Y. Luo, J. D. Sanchez-Yamagishi, K. Watanabe, T. Taniguchi, E. Kaxiras, R. C. Ashoori, P. Jarillo-Herrero, *Nature* **2018**, *556*, 80.
[123] Y. Cao, V. Fatemi, S. Fang, K. Watanabe, T. Taniguchi, E. Kaxiras, P. Jarillo-Herrero, *Nature* **2018**, *556*, 43.
[124] J. M. Park, Y. Cao, K. Watanabe, T. Taniguchi, P. Jarillo-Herrero, *Nature* **2021**, *590*, 249.
[125] H. Chen, X.-L. Zhang, Y.-Y. Zhang, D. Wang, D.-L. Bao, Y. Que, W. Xiao, S. Du, M. Ouyang, S. T. Pantelides, H.-J. Gao, *Science* **2019**, *365*, 1036.
[126] Y. Li, S. Dietrich, C. Forsythe, T. Taniguchi, K. Watanabe, P. Moon, C. R. Dean, *Nat. Nanotechnol.* **2021**, *16*, 525.
[127] C. Forsythe, X. Zhou, K. Watanabe, T. Taniguchi, A. Pasupathy, P. Moon, M. Koshino, P. Kim, C. R. Dean, *Nat. Nanotechnol.* **2018**, *13*, 566.
[128] R. Huber, M.-H. Liu, S.-C. Chen, M. Drienovsky, A. Sandner, K. Watanabe, T. Taniguchi, K. Richter, D. Weiss, J. Eroms, *Nano Lett.* **2020**, *20*, 8046.
[129] M. Yankowitz, J. Jung, E. Laksono, N. Leconte, B. L. Chittari, K. Watanabe, T. Taniguchi, S. Adam, D. Graf, C. R. Dean, *Nature* **2018**, *557*, 404.
[130] M. Yankowitz, S. Chen, H. Polshyn, Y. Zhang, K. Watanabe, T. Taniguchi, D. Graf, A. F. Young, C. R. Dean, *Science* **2019**, *363*, 1059.
[131] M. Kapfer, B. S. Jessen, M. E. Eisele, M. Fu, D. R. Danielsen, T. P. Darlington, S. L. Moore, N. R. Finney, A. Marchese, V. Hsieh, P. Majchrzak, Z. Jiang, D. Biswas, P. Dudin, J. Avila, K. Watanabe, T. Taniguchi, S. Ulstrup, P. Bøggild, P. J. Schuck, D. N. Basov, J. Hone, C. R. Dean, *Science* **2023**, *381*, 677.
[132] J.-B. Qiao, L.-J. Yin, L. He, *Phys. Rev. B* **2018**, *98*, 235402.
[133] X.-D. Chen, W. Xin, W.-S. Jiang, Z.-B. Liu, Y. Chen, J.-G. Tian, *Adv. Mater.* **2016**, *28*, 2563.
[134] Y. Saito, J. Ge, K. Watanabe, T. Taniguchi, A. F. Young, *Nat. Phys.* **2020**, *16*, 926.
[135] A. Uri, S. Grover, Y. Cao, J. A. Crosse, K. Bagani, D. Rodan-Legrain, Y. Myasoedov, K. Watanabe, T. Taniguchi, P. Moon, M. Koshino, P. Jarillo-Herrero, E. Zeldov, *Nature* **2020**, *581*, 47.
[136] A. Kerelsky, L. J. McGilly, D. M. Kennes, L. Xian, M. Yankowitz, S. Chen, K. Watanabe, T. Taniguchi, J. Hone, C. Dean, A. Rubio, A. N. Pasupathy, *Nature* **2019**, *572*, 95.
[137] T. E. Beechem, T. Ohta, B. Diaconescu, J. T. Robinson, *ACS Nano* **2014**, *8*, 1655.
[138] L. J. McGilly, A. Kerelsky, N. R. Finney, K. Shapovalov, E.-M. Shih, A. Ghiotto, Y. Zeng, S. L. Moore, W. Wu, Y. Bai, K. Watanabe, T. Taniguchi, M. Stengel, L. Zhou, J. Hone, X. Zhu, D. N. Basov, C. Dean, C. E. Dreyer, A. N. Pasupathy, *Nat. Nanotechnol.* **2020**, *15*, 580.
[139] S. Turkel, J. Swann, Z. Zhu, M. Christos, K. Watanabe, T. Taniguchi, S. Sachdev, M. S. Scheurer, E. Kaxiras, C. R. Dean, A. N. Pasupathy, *Science* **2022**, *376*, 193.
[140] H. Yoo, R. Engelke, S. Carr, S. Fang, K. Zhang, P. Cazeaux, S. H. Sung, R. Hovden, A. W. Tsen, T. Taniguchi, K. Watanabe, G.-C. Yi, M. Kim, M. Luskin, E. B. Tadmor, E. Kaxiras, P. Kim, *Nat. Mater.* **2019**, *18*, 448.
[141] D. Wang, G. Chen, C. Li, M. Cheng, W. Yang, S. Wu, G. Xie, J. Zhang, J. Zhao, X. Lu, P. Chen, G. Wang, J. Meng, J. Tang, R. Yang, C. He, D. Liu, D. Shi, K. Watanabe, T. Taniguchi, J. Feng, Y. Zhang, G. Zhang, *Phys. Rev. Lett.* **2016**, *116*, 126101.
[142] D. N. Theodorou, *Macromolecules* **1989**, *22*, 4578.
[143] M. Wang, M. Huang, D. Luo, Y. Li, M. Choe, W. K. Seong, M. Kim, S. Jin, M. Wang, S. Chatterjee, Y. Kwon, Z. Lee, R. S. Ruoff, *Nature* **2021**, *596*, 519.
[144] M. Nakatani, S. Fukamachi, P. Solís-Fernández, S. Honda, K. Kawahara, Y. Tsuji, Y. Sumiya, M. Kuroki, K. Li, Q. Liu, Y. C. Lin, *Nat. Electron.* **2024**, *7*, 119.
[145] S. Masubuchi, M. Morimoto, S. Morikawa, M. Onodera, Y. Asakawa, K. Watanabe, T. Taniguchi, T. Machida, *Nat. Commun.* **2018**, *9*, 1413.
[146] Qpress, https://www.bnl.gov/qpress/.